UCLouvain

FACULTE DES SCIENCES

Faculté des sciences

Synthesis and characterization of polymer electrolytes with a vitrimer behaviour

Author: Oriane Froment

Supervisor: Pr. Jean-François Gohy

Readers : Pr. Charles-André Fustin
Pr. Tom Leyssens
Pr. Alexandru Vlad

Academic year 2022-2023

Master [120] en sciences chimiques, à finalité spécialisée: chimie de l'industrie

Acknowledgments

First of all, I would like to express my gratitude to my supervisor, Professor Jean-François Gohy, who accepted me into his research group and shared his valuable expertise on batteries with me. He made me discover the wonderful research topic of solid polymer electrolyte (mixing polymer and battery chemistry).

Then, I could not have undertaken this journey without Carla Barakat, who helped me so much during the experimental work and the redaction of this master thesis. She was always there to answer my questions and guide me through the research. Moreover, her enthusiasm and generosity always kept me motivated.

I am also grateful to the readers, Professors Charles-André Fustin, Tom Leyssens and Alexandru Vlad, for being part of my jury. Thank you for the time invested in reading this master thesis.

Lastly, I had the pleasure of working with the research group of the wing B2. All the members were kind and helpful (giving useful advice and lending me Teflon mould). Additionally, they would create a good working environment with after-work drinks and games.

Abstract

Lithium-ion batteries are ubiquitous in our daily lives and their demand is increasing drastically to tackle the climate change by electrifying transportation and accelerating clean power generation. However, the use of lithium-ion batteries in electric vehicles and its other applications raises safety issues while the need of batteries with higher energy density grows stronger. Therefore, the development of lithium-metal batteries aims to solve the current problems of lithium-ion batteries. A functional lithium-metal batteries can be obtained with a solid-state electrolyte. The focus of this master thesis will be on solid polymer electrolyte, which is a type of solid-state electrolyte, for lithium-metal batteries. That solid polymer electrolyte has a vitrimer behaviour to minimize some problems faced with solid-state electrolyte in lithium-metal batteries (such as cracks appearing and dendrite formation). To put it simply, a vitrimer is a polymer network with interesting properties such as shape memory and self-healing. The aim of this work is to synthesize and characterize a solid polymer electrolyte with a vitrimer behaviour for lithium-ion batteries. The ionic conductivity of that solid polymer electrolyte will be improved by changing the crosslinking density and the crosslinker molar mass of the polymer network.

Table of content

List of Abbreviations

Abbreviation	Definition
CAN	Covalent adaptable network
CE	Coulumbic efficiency
CEI	Cathode electrolyte interface
DMAP	4-dimethylaminopyridine
DSC	Differential scanning calorimetry
EU	European Union
EV	Electric vehicle
ICE	Inorganic ceramic electrolyte
LCO	Lithium cobalt oxide
LIB	Lithium-ion battery
mL	Milliliter
NCA	Lithium nickel cobalt aluminium oxide
NiMH	Nickel metal hydride
NMC	Lithium nickel maganese oxide
OM	Optical microscopy
PEGDE	Polyethylene gycol diglicyl ether
PEIS	Potential electrochemical impedance spectroscopy
SCE	Solid composite electrolyte
SEI	Solid electrolyte interface
SPE	Solid polymer electrolyte
SSE	Solid-state electrolyte
TBP	n-tributyl phosphine
T_D	Degradation temperature
T_g	Glass transition temperature
TGA	Thermo gravimetric analysis
THF	Tetrahydrofuran
wt %	Weight percentage

List of figures

List of tables

List of graphs

1. Introduction

"An electric bus caught fire after battery explosion in Paris" [1]

Such headlines are not uncommon in the news since at least 25 000 incidents of fire or overheating in lithium-ion batteries (LIB) occurred over a recent five-year period [2]. As you might know, LIBs are widely used in portable electronics, such as computers and cell phones, but also for electric or hybrid vehicles [3]. The LIBs are quite popular because of their high energy density, long cycle life, and low self-discharge rate compared to other types of batteries [4]. In fact, they are so popular that the global sales of electric vehicles reached 4 million in 2020 and is estimated to 245 million in 2030 [5]. Such an exponential demand in electric vehicles, is mainly due to new regulations involving combustion vehicles. Indeed, the European union (EU) aims to reduce net greenhouse gas emissions by at least 55% in 2030, compared to 1990 levels [6]. To attain this goal, all diesel engines will be banned in Brussels from 2030 and petrol cars from 2035 [7]. A similar law should be passed in the EU, leading to a gradual replacement of combustion engine vehicles by electric vehicles.

However, the use of LIB in electric vehicles and its other applications raises a lot of concerns in respect to safety. Fire and explosion accidents occurred regularly, leading to tons of LIBs being recalled [3]. Usually, a commercial LIB is composed of an anode, a cathode, a separator, and a liquid electrolyte. That electrolyte may induce some serious hazards due to the flammability and easy ignition of the organic solvents used in the liquid electrolyte [8].

Different strategies such as flame-retardant additives, ionic liquids, and solid-state electrolytes (SSE) emerged to improve the safety of LIBs. Replacing the liquid electrolyte by a non-flammable SSE is an appealing solution because electrolyte leakage and flammability at high temperature are not problematic when using SSEs. But SSEs also offer the potential to dramatically improve the energy density of batteries by replacing the graphite anode with lithium-metal.

In this master thesis, the focus will be on solid polymer electrolyte, one type of SSE, for lithium-metal batteries. To improve some problems faced with classical SSEs such as cracks appearing due to volume changes or dendrite formation, that solid polymer electrolyte has a vitrimer behaviour, meaning that the polymer has self-healing abilities.

As solid polymer electrolytes have a lower ionic conductivity than liquid electrolytes, the aim of this master thesis is to optimize the ionic conductivity of the solid polymer electrolyte with a vitrimer behaviour by changing the molar mass of the crosslinker and the crosslinking density of the polymer network.

In chapter 2, the theoretical background on LIB, lithium-metal batteries, solid state electrolytes and vitrimers will be explained. The chapter 3 will focus on the synthesis and film formation of the solid polymer electrolyte. Lastly, the results will be exposed in chapter 4 with an electrochemical, structural and thermal characterisation.

2. Theoretical background

Before diving into the experimental part of this master thesis, some key concepts and notions will be explained. Knowledge such as lithium-ion batteries, solid-state electrolyte, and vitrimer chemistry will be detailed in the theoretical background.

2.1.Lithium-ion batteries

2.1.1. Primary and secondary batteries

A battery is a device composed of two or more electrochemical cells capable of converting chemical energy directly into electrical energy with redox reactions [9]. Batteries can be separated in two categories depending on the reversibility of the redox reactions. Primary batteries can only be used once, until the chemicals producing electricity are depleted. The electrochemical reactions occurring in the battery are irreversible, making it impossible to recharge the battery. Primary cells are often used to power small household and consumer devices like flashlights and portable radios. On the contrary, secondary batteries can be charged and discharged multiple times thanks to the reversibility of the redox reactions. Secondary batteries are mainly used in portable electronic devices such as laptops, mobile phones, hearing aids, and watches, as well as in EVs and electricity grid networks [10].

$$Electrical\ energy \overset{redox\ reaction}{\longleftrightarrow} Chemical\ energy$$

2.1.2. Working principle of lithium-ion batteries

2.1.2.1. General principle

An electrochemical cell can be simplified as a system containing two dissimilar electrodes dipped in an electrolyte (substance transporting ions). The electrode with the lower affinity for electrons becomes positively charged by giving away electrons to the one with the higher affinity, which turns into a negatively charged electrode. A potential difference is thus created between the two electrodes, and if they are connected by wires, electrons will start flowing from one electrode to the other, producing electricity. This process is called discharging. Secondary batteries can be charged back by applying a negative potential, and the electrons are retraced back to their original electrode. The negative electrode is called the

anode on the discharge, and cathode on the charge, whereas the positive electrode is called the cathode on the discharge and anode on the charge. The anode is always where the oxidation reaction occurs, while the reduction happens on the cathode [11].

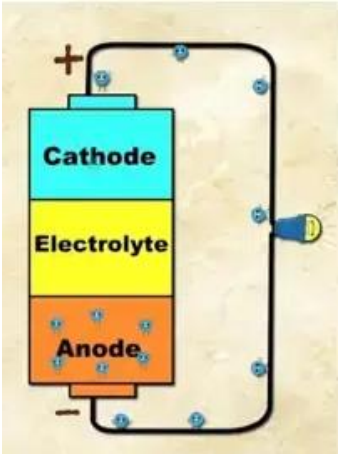

Figure 1: Discharge of an electrochemical cell [12]

2.1.2.2. Lithium-ion batteries

Batteries have more than 200 years of history. In 1800, Allesandro Volta successfully demonstrated a modern battery that could continuously provide an electric current to a circuit. Since then, different types of batteries emerged, at first primary batteries, such as the Daniell cell, the Leclanche cell, and the most commonly used nowadays: the alkaline cell. Then secondary batteries were developed with lead-acid, nickel-cadmium, nickel metal hydride (NiMH), and lithium-ion batteries (LIB) [13]. Nowadays, LIB is the most popular type of secondary battery, widely used in portable devices, electric vehicles, and grid storage. Such a popularity is due to a high energy density, high power density, and long cycle life possessed by LIB. Why is lithium so interesting in LIB? Simply because lithium is the lightest and most electropositive metal, giving thus a high energy density [14]. Obviously, LIB provides power through the movement of lithium ions. Let us take a quick look at the working principle of LIB before detailing the main components found in such a battery.

Lithium-ion batteries have 4 main components: a positive electrode made of lithium metal oxide, a negative electrode usually made of graphite, a separator preventing direct contact between the two electrodes and an electrolyte which is a solvent transporting lithium-ions from one electrode to the other when the battery is used.

When the battery is being discharge, the lithium ions deintercalated from the graphite electrode (liberating one electron) and travel to the metal oxide electrode through the

electrolyte. On the positive electrode side, the lithium ion is intercalated in the metal oxide structure, using one electron for this reaction. The redox reactions occurring at the electrodes are described in Equation 1.

Equation 1: Reactions during LIB discharge

Negative electrode (***oxidation***): $LiC_6 \rightarrow Li^+ + e^- + C_6$

Positive electrode (**reduction**): $MO_2 + Li^+ + e^- \rightarrow LiMO_2$

When charging the battery, the lithium ions will go back to the graphite electrode, and the reactions are this time reversed with the reduction occurring at the negative electrode and the oxidation at the positive electrode [15].

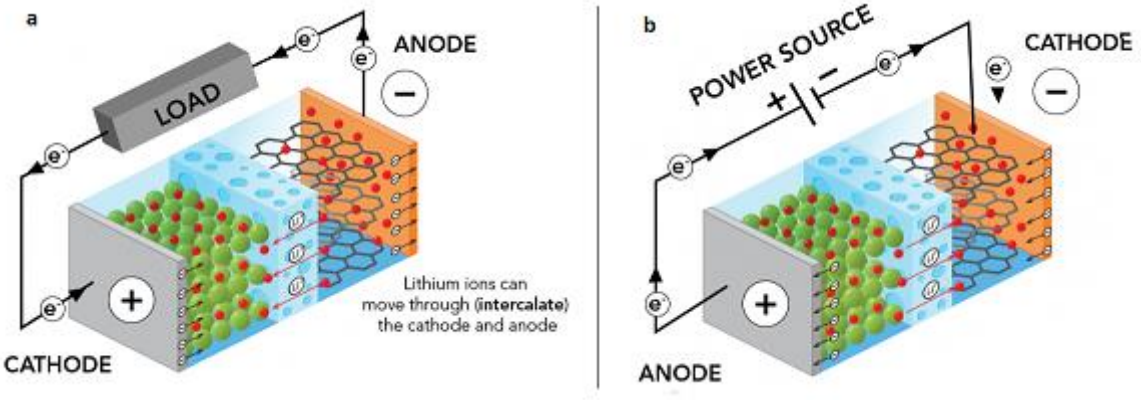

Figure 2: Discharge of LIB (a) and charge (b) [15]

2.1.2.3. Components in lithium-ion batteries

A LIB is composed of a positive electrode (cathode), a negative electrode (anode), a separator, an electrolyte and two current collectors (Figure 3). The chemistry behind these different components will be detailed below.

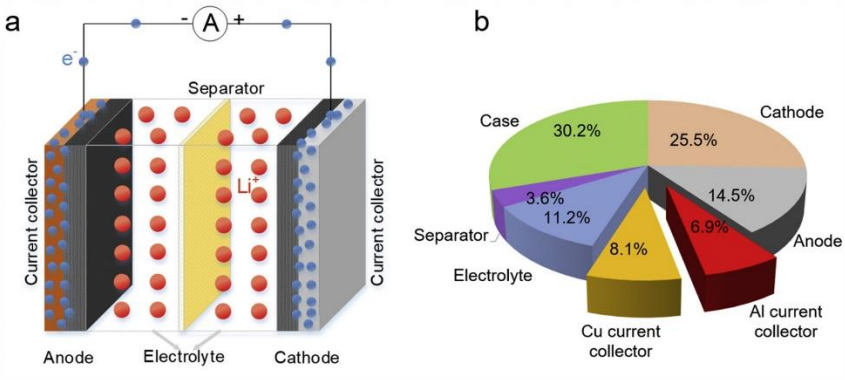

Figure 3: Typical lithium-ion battery (a) and the weight percentages of its main components (b) [16]

2.1.2.4. Current collectors

The purpose of current collectors is to collect electrical current generated at the electrodes and connect that current with external circuits. Commercial current collectors are aluminum (Al) and copper (Cu) foils for positive electrodes and negative electrodes, respectively [17]. The same current collector cannot be used for both electrodes due to the potential stability window of the materials. Indeed, Al is not stable at lower potential in LIB, and is thus used at the positive electrode side (cathode). Copper, on the other hand, is employed at the negative electrode side (anode) as it does not involve redox reaction at lower potential.

2.1.2.5. Negative electrode

The negative electrode should have the lowest potential, a high capacity, and be stable. Graphite is the most commonly used material for the negative electrode as it possesses a voltage close to 0,1 Volt. Lithium ions are intercalated between the layers of graphite. On the negative electrode side, the formation of an effective solid electrolyte interface (SEI) is necessary to avoid the co-intercalation of solvent, and thus the exfoliation of graphite. The SEI is an insulating layer on the electrode, letting the lithium ions pass through but not the solvent and anion. The SEI is formed during the first charge of the battery by the decomposition of organic solvents and lithium salts.

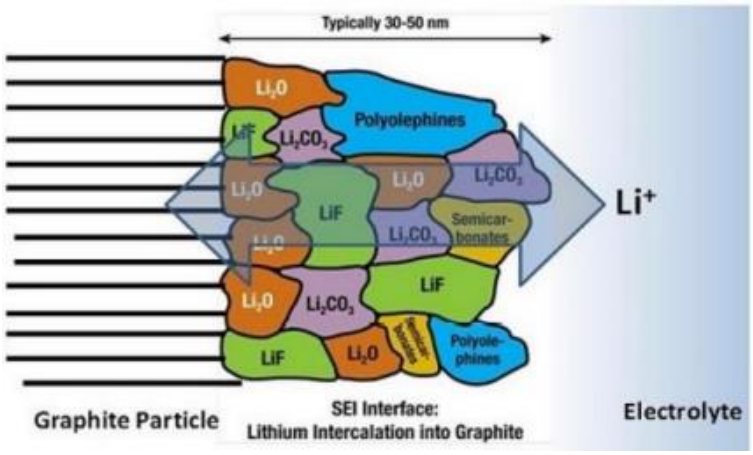

Figure 4: Solid electrolyte interface [13]

2.1.2.6. *Positive electrode*

The positive electrode is a solid host network, which can store lithium ions reversibly. Different types of positive electrode materials can be used as solid host networks. The most common materials for commercial LIB are lithium cobalt oxide (LCO or $LiCoO_2$), lithium manganese oxide (LMO or $LiMn_2O_4$), lithium iron phosphate (LFP or $LiFePO_4$), lithium nickel manganese cobalt oxide (NMC or $LiNi_xCo_yMn_zO_2$) and lithium nickel cobalt aluminum oxide (NCA or $LiNi_xCo_yAl_zO_2$). Each of these lithium metal oxides has its advantages and drawbacks, but LCO, the most used positive electrode material, is slowly being replaced by NMC and NCA on the market [18]. A comparison of these different solid host networks is shown in Figure 5.

Cathode types	LCO	LMO	LFP	NCA	NMC
Chemical formula	$LiCoO_2$	$LiMn_2O_4$	$LiFePO_4$	$LiNi_xCo_yAl_zO_2$	$LiNi_xCo_yMn_zO_2$
Structure	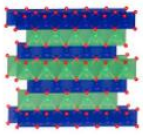	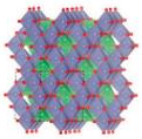	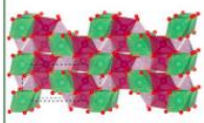	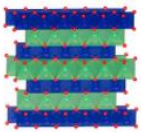	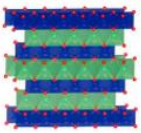
Market share	Dumped	Small	Growing	Steady	Main force
Typical use	Portable electronic devices	Power tools and electric bikes	Electric bikes, large EVs and power tools	Panasonic batteries for Tesla EVs	Portable electronic devices and EVs
Comments	Low safety, high cost, medium performance	Medium safety, low cost, medium energy density, low lifetime	Good safety, low cost, high thermal stability, medium energy density	Medium safety, medium cost, higher energy density	Medium safety, medium cost, higher energy density, high lifetime

Figure 5: Comparison of positive electrode materials in commercial LIB [18]

Similar to the SEI for the negative electrode, a passivation film (called CEI) is formed on the positive electrode with the oxidation of electrolyte solvents and salts.

2.1.2.7. *Separator*

A separator is a thin polymeric film preventing the direct contact between the negative electrode and the positive electrode. Without a separator, the direct reaction would take place, resulting to the short-circuit of the cell. The separator is an electrical insulator but an ionic conductor, letting the lithium ions through. Common commercial separators found in LIB are composed of polyethylene and polypropylene in the form of microporous membranes [19].

2.1.2.8. Electrolyte

Like the separator, the electrolyte is also an electrical insulator and an ionic conductor. The purpose of the electrolyte is to dissolve the lithium ions and transport them to the other electrode. In most commercial LIB, a liquid electrolyte composed of organic solvents is used. Those organic solvents should have a high dielectric constant to dissolve efficiently the lithium ions (and prevent the formation of aggregates) but also a low viscosity to rapidly transport the lithium ions. Thus, mixtures of carbonate solvents with high dielectric constant and low viscosity are found in commercial LIB with a ratio optimizing the ionic conductivity. A common example of those carbonate solvents is ethylene carbonate (EC), possessing a high dielectric constant, combined with dimethyl carbonate (DMC) or ethyl methyl carbonate (EMC) or diethyl carbonate (DEC), which are solvents with a low viscosity.

The solvents found in a liquid electrolyte are volatile and highly flammable. Under normal circumstances, this does not cause any problems. However, in case of short-circuit (due to manufacturing defects or mishandling of the battery), the cell would overheat, leading to the liquid electrolyte spontaneously catching fire. This causes serious threats to human health and life.

Other than the solvents, the electrolyte also contains lithium salts and additives. The lithium hexafluorophosphate ($LiPF_6$) is found in most commercial batteries as it has the best compromise between ionic mobility and dissociation constant. Other lithium salts have a better ionic conductivity (like $LiClO_4$ and $LiBF_4$) but a worse constant dissociation than $LiPF_6$ or a worse ionic conductivity but better dissociation constant (like $LiAsF_6$ and LiTFSI).

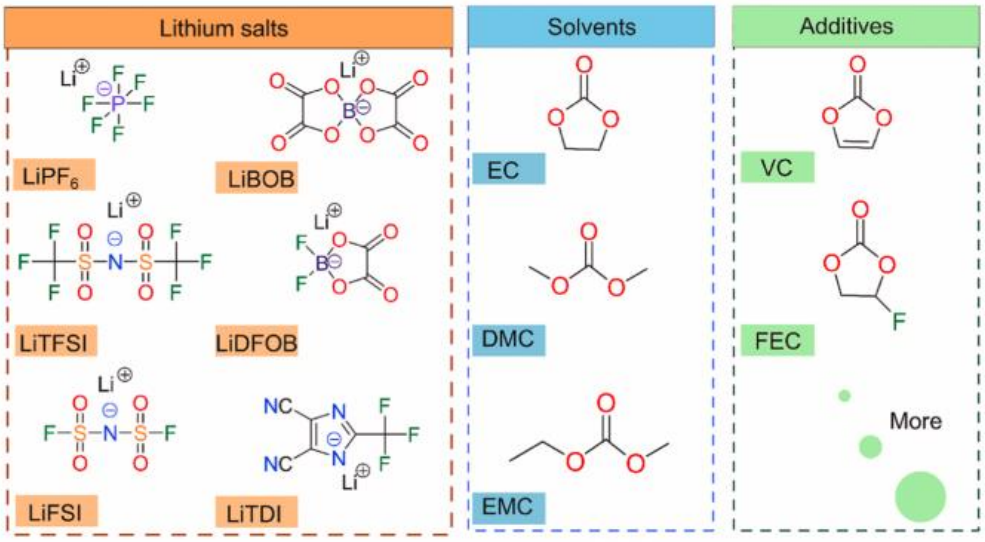

Figure 6: Liquid electrolyte composition in LIB [13]

Two types of additives can be found in the electrolyte: film forming additives and functional additives. The film forming additives will help to form the SEI and/or the CEI. Functional additives could be salt dissociation promotors, flame-retardants, corrosion inhibitors, and so on.

Until now, we saw the working principle of the most popular commercial battery, the lithium-ion battery. The main components inside LIB are graphite (negative electrode), metal oxide (positive electrode) and a mixture of organic solvents, lithium salts as well as additives (electrolyte). Even though LIBs are used for many applications and have good performances (energy density, power density, and cycle lifetime), some limitations become apparent. Taking the example of electric vehicles, only about 2% of new car sales in the US are EV and just a little more globally. Many buyers still prefer fuel cars for economic reasons (cost) or because they find the range of EV too limited and charging them is slower and less convenient than refuelling at the pump. All these limitations are related to the fact that LIBs are costly, heavy, and quick to run out of juice. To make matters worse, the LIB contains highly flammable solvents in the electrolyte that can burst into flames during collisions [20]. The development of lithium-metal batteries aims to solve the current problems of lithium-ion batteries. What are lithium-metal batteries exactly? Let us take a look at the next generation of battery with lithium.

2.1.3. Towards lithium-metal batteries

The idea behind lithium-metal batteries is quite straightforward: replacing the graphite of the negative electrode directly by lithium metal. Indeed, graphite is merely a host for the lithium ions, it doesn't store energy or produce a current itself. In other words, the graphite is a dead weight in the battery, adding weight without producing any current. In a lithium-metal battery, the negative electrode itself is made from lithium. Theoretically, nearly every lithium atom in the battery negative electrode can be put to work creating current. Thus, a lithium-metal battery could store more energy than a lithium-ion battery of the same weight and volume.

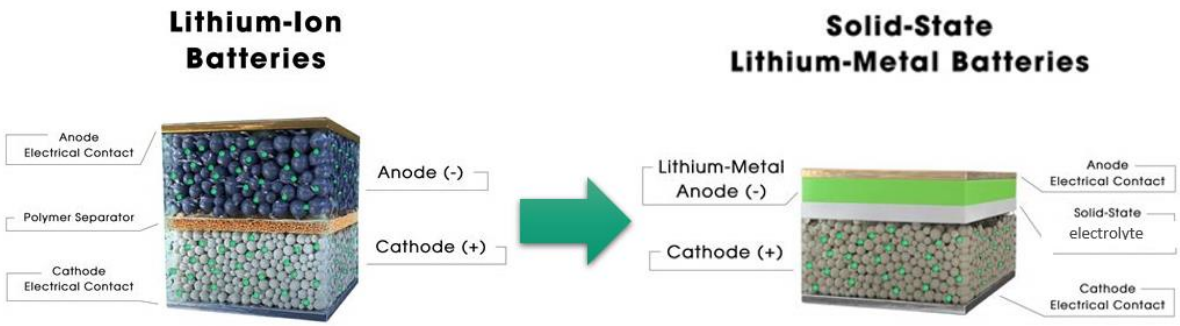

Figure 7: Comparison of LIB and lithium-metal batteries [21]

Now, lithium-metal batteries might sound wonderful to you but do not be deceived, those batteries also have many challenges. The main problem of lithium-metal batteries with a liquid electrolyte is the formation of harmful lithium dendrites.

Dendrite formation is common for metal electroplating at higher currents. In lithium-metal batteries, the lithium needs to be plated and stripped repeatedly during charge/discharge processes. After a few cycles, dendrites with needle-like, mossy-like, or branch-like structures will appear on the surface of lithium negative electrodes. These dendrites can pierce the separator to reach the positive electrode, causing the short circuit. Thermal runaway usually accompanies short circuits, but it could even cause spontaneous combustion and explosion. To sum up, lithium-dendrites causes serious safety issues.

Another problem with lithium-metal batteries is that lithium dendrites are quite reactive, leading to side reactions with the liquid electrolyte. Those side reactions can consume both metallic lithium and the electrolyte, destroying dendrites but forming an insulating layer around the lithium metal, which is called "dead lithium". The consumption of lithium metal

on the negative electrode will result to a loss of active material, causing a decrease in Coulombic efficiency (CE) and cycle life of the battery [22].

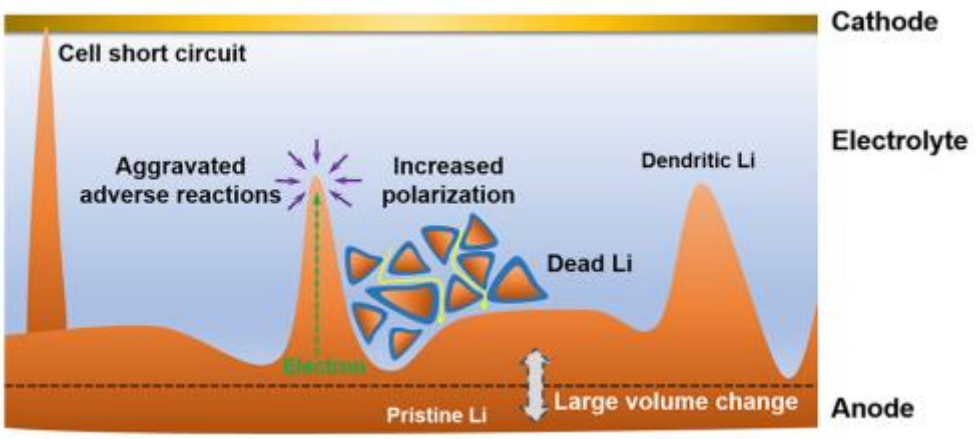

Figure 8: Lithium dendrite formation in lithium-metal batteries [23]

To tackle the challenges faced by lithium-metal batteries, different strategies have been developed, such as the modification of the separator, new additives in the liquid electrolyte or solid-state electrolytes (SSE). That last strategy, consist of replacing the liquid electrolyte by a solid electrolyte. It would prevent (or at least minimize) lithium dendrite growth and avoid several safety issues existing in batteries with liquid electrolytes, such as leakage, flammability, and poor chemical stability. Another point to consider after the replacement of liquid electrolytes by solid ones in lithium-metal batteries is the ionic conductivity inside the cathode materials. Indeed, liquid electrolytes are diffusing into the porosity of the cathode materials and ensure Li-ion transfer in/out the cathode. In case of use of solid electrolytes, those ones need to be pre-mixed with the other cathode components during electrode fabrication. This gives rise to the so-called catholyte concept.

Are you convinced by the use of SSE to face the challenges of lithium-metal batteries? In any case, solid state electrolytes will be the topic of the next section as this master thesis is focused on solid polymer electrolyte (a type of SSE that you will discover later on).

2.2. Solid-state electrolyte

2.2.1. Types of solid-state electrolytes

In the previous section, we saw that SSE could be used in lithium-metal batteries to prevent (or at least minimize) the formation of dendrites and improve the safety of such a

battery. But SSE can also help with the safety of LIB by replacing the highly flammable and volatile organic solvents by a non-flammable solid state electrolyte. Solid-state electrolytes can be divided into three classes: inorganic ceramic electrolytes (ICE), solid polymer electrolytes (SPE) and solid composite electrolytes (SCE). To fulfil the same purpose as liquid electrolytes, SSE should possess several characteristics which are a high ionic conductivity (> 10^{-4} $S.cm^{-1}$), good mechanical properties to resist to the penetration of dendrites and flexibility to maintain a good contact with the electrodes during battery operation, negligible electronic conductivity, large electrochemical stability window as well as a good transfer between interfaces (SSE-electrode). Fulfilling all these requirements is not an easy task, thus, the advantages and drawbacks of each type of SSE will be explained [24].

2.2.2. Inorganic ceramic electrolytes

Inorganic ceramic electrolyte transport lithium ions trough the lattice. Some examples of ICE are perovskite, garnet, sodium super-ionic conductors (NASICON) and sulfide-type materials. A high ionic conductivity is obtained with ICE (> 10^{-3} $S.cm^{-1}$ at room temperature). However, ICEs are difficult to process and have poor interfacial contact due to the lack of flexibility. Also, ceramics are brittle, which leads to the formation of cracks in the ICE caused by the volume change of the electrodes during the charge/discharge process [25].

2.2.3. Solid polymer electrolytes

Solid polymer electrolytes (SPE) possess many advantages compared to liquid electrolytes, including the lack of leakage, low flammability, safety, great flexibility, and easy processing. However, the ionic conductivity of SPE is quite low at room temperature compared to liquid electrolytes (10^{-4}-10^{-6} $S.cm^{-1}$).

SPE are often based on poly(ethylene oxide) (PEO) as host matrix. PEO can dissolve the lithium salt and conduct the lithium ions thanks to the coordination of oxygen atoms with the lithium ions. The ionic transport occurs through an oxygen assisted hopping of the ions from site to site and the movement of the polymer chain.

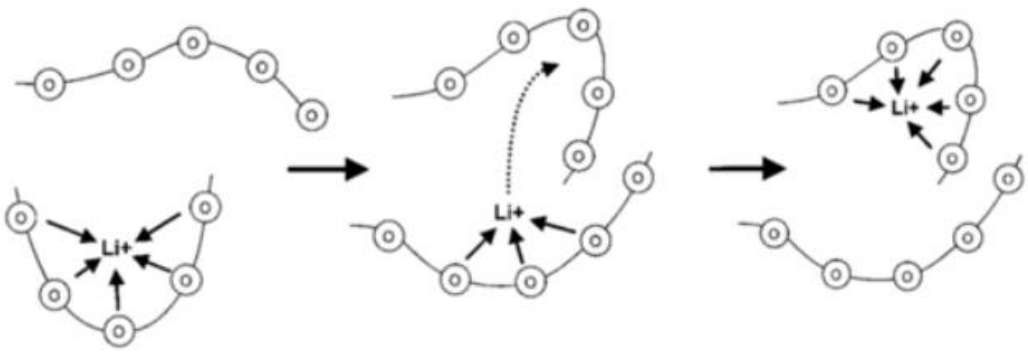

Figure 9: Mechanism of ion transport in PEO [26]

In fact, the movement of polymer chains is closely related to the glass transition temperature (T_g) and the crystallinity of that polymer. At a temperature higher than T_g, the movement of the chains will improve, resulting to a higher ionic conductivity. In crystalline regions, the ionic conductivity reaches $\leq 10^{-6}$ S.cm^{-1} while this number rises to $>10^{-4}$ S.cm^{-1} for amorphous regions above T_g. To improve the ionic conductivity of SPE, the presence of crystalline domains should thus be reduced [27].

2.2.4. Solid composite electrolytes

Solid composite electrolytes (SCE) are composed of a polymer matrix with inorganic nanoparticles. This electrolyte is a hybrid between ICE and SPE. The ionic conductivity of SCE is usually between 10^{-3} and 10^{-4} S.cm^{-1} but this number is highly dependent on the weight fractions of the ceramic and the surface area of the fillers. Another drawback of solid composite electrolytes is the high interfacial resistance between the electrode and the electrolyte, but also between inorganic particles and the polymer matrix. That high interfacial resistance results to an overall poor ionic conductivity [28].

2.2.5. Comparison of the different SSEs

To sum up, each type of SSE has their advantages but also their drawbacks. A high ionic conductivity and good transfer at the interface are often difficult to obtain together. Compromises must be made between a high ionic conductivity (for ceramic and composite electrolytes) or transfer at the interface and resistance to volume change (for polymer electrolytes.

Inorganic ceramic electrolyte	Solid polymer electrolyte	Solid composite electrolyte
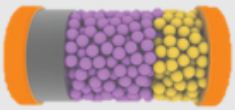	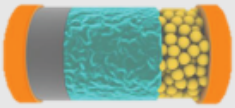	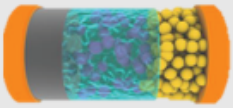
✓ High ionic conductivity ($\sim 10^{-3}$ S.cm^{-1})	✓ Resistance to volume changes ✓ Stability at the interface	✓ Advantages of both types
✗ Brittle ✗ High interfacial resistance	✗ Low ionic conductivity ($\sim 10^{-5}$ S.cm^{-1}) ✗ Limiting fast-charging	✗ Still a low ionic conductivity ✗ High interfacial resistance

Figure 10: Advantages and drawbacks of the different SSEs

The focus of this master thesis will be on solid polymer electrolytes for application in lithium-metal batteries. The polymer used as SPE in this work shows a vitrimer behaviour. In the next section, the advantages of using that type of polymer in SPE will be explained, followed by the characteristics of vitrimers.

2.3. Vitrimers chemistry

2.3.1. Covalent adaptable networks (CANs)

2.3.1.1. Thermosets, thermoplastics, and CANs

To explain what vitrimers are, we need to look at the broader picture with the classes of polymers and covalent adaptable networks. Thermoplastics and thermosets are two main classes of polymers. Common examples of thermoplastics are poly-(styrene), poly(ethylene), poly(ethylene terephthalate), and poly(vinyl chloride). They can be melted and reprocessed at elevated temperature. Thermoplastics can thus be recycled and reprocessed. On the other hand, thermosets cannot be recycled after their initial processing, but they have a higher mechanical strength, as well as thermal and chemical stability compared to thermoplastics. Some examples of thermosets are melamine resins, epoxy resins, silicone resins, and urea formaldehydes. Those different properties between thermosets and thermoplastics are, in fact, explained by their chemical structure. Thermoplastics are composed of linear polymeric chains while thermosets comprise three-dimensional networks with covalent links. Those covalent crosslinks cannot be easily broken even at high temperatures, and the polymer usually decomposes before melting. Recently, a new class of polymers with properties in

between thermosets and thermoplastics was discovered. This class is called covalent adaptable networks (CANs) [29].

2.3.1.2. Vitrimers

CANs are polymer networks containing dynamic covalent bonds. These bonds are dynamic under specific conditions and can undergo bond exchange. Without stimulus, the polymeric materials act as a thermoset, with properties such as strength and durability. But, unlike thermosets, CANs are recyclable due to the dynamic nature of their crosslinks. In presence of a stimulus (heat, catalyst, light or pH), the covalent crosslinks become dynamic covalent bonds. Furthermore, CANs can exhibit properties like malleability, shape memory, and self-healing [29].

CANs can be divided into two subgroups depending on mechanism taking place during the bond exchange: dissociative and associative mechanisms.

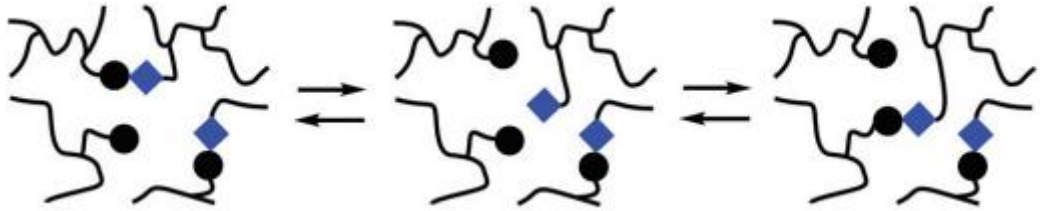

Figure 11: CANs dissociative mechanism [30]

Most CANs undergo a dissociative mechanism where the crosslinking bonds break down before forming new bonds (Figure 11). On the other hand, the crosslinks are only broken when new bonds are formed in the associative mechanism. The crosslink density of associative CANs is considered to be almost constant regardless of external stimuli (Figure 12).

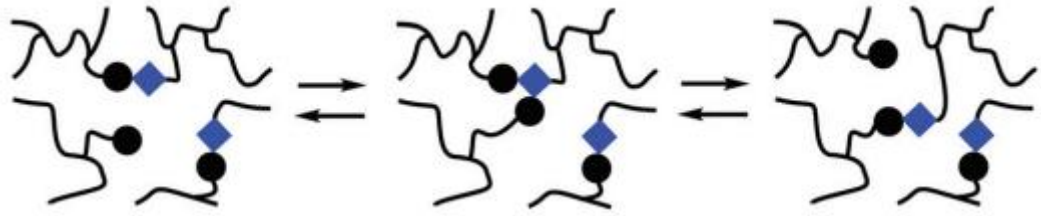

Figure 12: CANs associative mechanism [30]

CANs with an associative mechanism are called vitrimers. They are characterized by a gradual decrease in the viscosity when the temperature increases. The chemical bonds cannot easily be classified based on the mechanism (associative/dissociative) as some chemical bonds can do both mechanisms depending on the conditions. Moreover, some CANs with a dissociative mechanism may have rheological properties identical to vitrimers [31]. A viscosity-temperature dependence like CANs with associative mechanism is observed in these materials. This type of material, called vitrimer-like, is obtained when the rate constant of bond formation is significantly higher than that of bond cleavage. Vitrimeric materials possess intriguing properties such as re-processibility and recyclability, but also shape-memory, malleability and self-healing. Numerous applications with vitrimeric materials are now explored. Obviously, one of these applications, is the use of vitrimeric materials as solid polymer electrolyte for LIB and lithium-metal batteries.

2.3.2. Self-healing solid polymer electrolyte

The use of vitrimeric materials in SPE will bring many advantages such as improving the cycle lifetime and safety. First of all, the volume change of the electrodes can shorten the battery's lifetime due to cracks appearing after repeat charge/discharge. Even though SPE are more resistant to volume changes than ICE, cracks will still form after several cycles. But with a self-healing material (like vitrimeric materials), cracks in the SPE could heal themselves, thus improving the lifetime of the battery after cracks or deformations. Secondly, the safety of lithium-metal batteries could be improved with a vitrimeric SPE. Indeed, the dendrite formation can be slowed down by the self-healing of the SPE, therefore improving the safety of lithium-metal batteries by preventing short-circuits [32].

2.3.3. Disulfide (S-S) bond exchange

Different chemical bonds can give vitrimer or vitrimer-like properties such as esters, carbamate, carbonate, carbamide, acetal, disulfide, and so on. But the SPE of this work is based on disulfide bond exchange in a polysulfide network to obtain a vitrimer behaviour. The disulfide metathesis is the rearrangement of sulfur-sulfur bonds. These bonds are thus dynamic covalent bonds. Disulfide bond exchange usually undergoes a dissociative mechanism and does not exhibit a vitrimer behaviour under normal circumstances. However, with a catalyst, a vitrimer behaviour can be observed in a network with disulfide bonds [33].

A nucleophile such as tri-nbutylphosphine (TBP) is added as catalyst to favour the disulfide metathesis, even at room temperature. The disulfide bond exchange reaction proceeds via thiolate anions, generated by the reduction of the disulfides. The catalyst-assisted dissociative mechanism is shown in Figure 13. With the catalyst, the polysulfide network possesses a vitrimer behaviour, and properties such as self-healing can be observed.

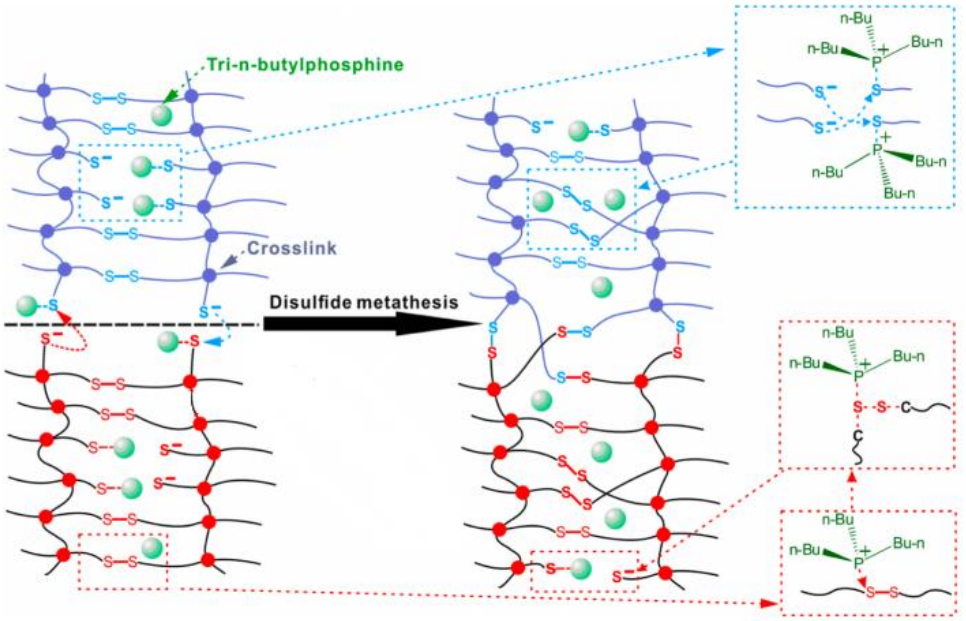

Figure 13: TBP-catalysed disulfide metathesis in a polysulfide network [34]

3. Experimental part

In the theoretical background, the working principle and different components of LIBs were detailed. LIBs are ubiquitous in our daily lives, but some limitations of LIBs push towards the development of lithium-metal batteries. These new generation batteries have a high energy density thanks to the lightness and high voltage of lithium-metal. However, the formation of lithium dendrites causes huge challenges related to safety and cycling stability. To solve those problems, the traditional liquid electrolyte should be replaced by a solid-state electrolyte in lithium-metal batteries. Among the different solid-state electrolytes, solid polymer electrolytes show a good electrolyte/electrode interface, owing to the flexibility of polymers.

But the low ionic conductivity (10^{-4} – 10^{-6} $S.cm^{-1}$) is the major drawback of SPEs. Moreover, SPEs may still suffer from dendrite penetration that could cause irreversible damage to the battery. Although SPEs are flexible materials, the SPE/electrode interfacial contacts could also be disrupted as a result of the electrode volume changes experienced during battery cycling.

Vitrimers and vitrimer-like materials are networks with dynamic covalent bonds, where the viscosity decreases gradually as the temperature increases. Such materials can be reprocessed, have shape-memory and can self-heal. Thus, they make ideal candidates as polymer for SPE. Using vitrimers or vitrimer-like materials in SPE would improve the cycling lifetime and safety of the battery, thanks to the self-healing of the polymer network. A vitrimer-like material can be obtained with a catalysed disulfide metathesis in a polysulfide network. This type of network will be the topic of this work.

In other words, this research is on the synthesis and characterisation of solid polymer electrolytes with a vitrimer behaviour obtained via a catalysed disulfide metathesis. That solid polymer electrolyte could be used in LIBs to improve their safety as well as in lithium-metal batteries where liquid electrolytes cannot be employed due to safety issues. Now that you certainly have understood the title of this master thesis, let’s look at the chemistry behind the polysulfide network used as SPE.

3.1. Polysulfide network formation

3.1.1. Thioplast G131

The base polymer to prepare the polysulfide network is a Thioplast G131 produced by AkzoNobel. The chemical structure of the thioplast G131 is shown in Figure 14.

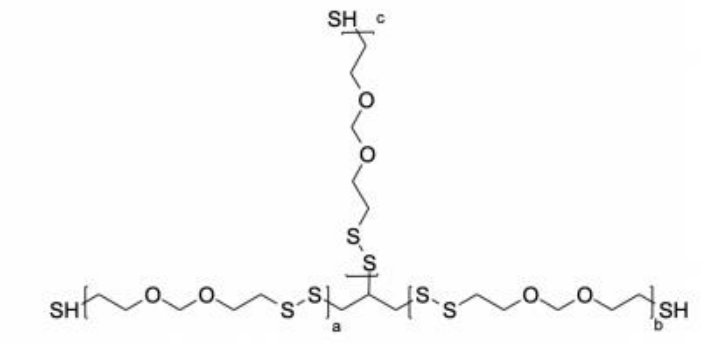

Figure 14: Thioplast G131 (a + b + c = 31-38)

The technical characteristics of the thioplast G131 are summarised in Table 1.

Table 1: Technical characteristics of the thioplast G131

	Units	**Thioplast G131**
Average MW	g/mol	5200 - 6500
SH content relatively to MW	wt%	1 – 1,3

This thioplast was selected as base polymer because it satisfied the requirements needed to obtain an SPE with a vitrimer behaviour. Those requirements are:

1) The presence of oligoethylene oxide in the polymer backbone to dissolve and transport the lithium ions through coordination and hopping mechanism.
2) The presence of disulfide bonds induces vitrimer-like properties via the disulfide metathesis [35].
3) The thiol-end groups are used to form a network via nucleophilic addition reaction.

3.1.2. Crosslinking reaction

To obtain a vitrimer behaviour, a network with dynamic covalent bonds should be formed. Poly(ethylene glycol) diglycidyl ether (PEGDE) was chosen as crosslinker so that the thioplast is chemically crosslinked via a thiol-epoxy nucleophilic addition reaction. PEGDE also possess an oligo(ethylene oxide) in the polymer backbone, helping with the dissolution

and transport of lithium ions. The crosslinking reaction shown in Figure 15 is promoted by 1 wt% of 4- dimethylaminopyridine (DMAP). Moreover, 0,3 wt% of n-tributylphosphine (TBP) are added as catalyst for the disulfide metathesis. A polysulfide network with a vitrimer behaviour is obtained after this crosslinking reaction.

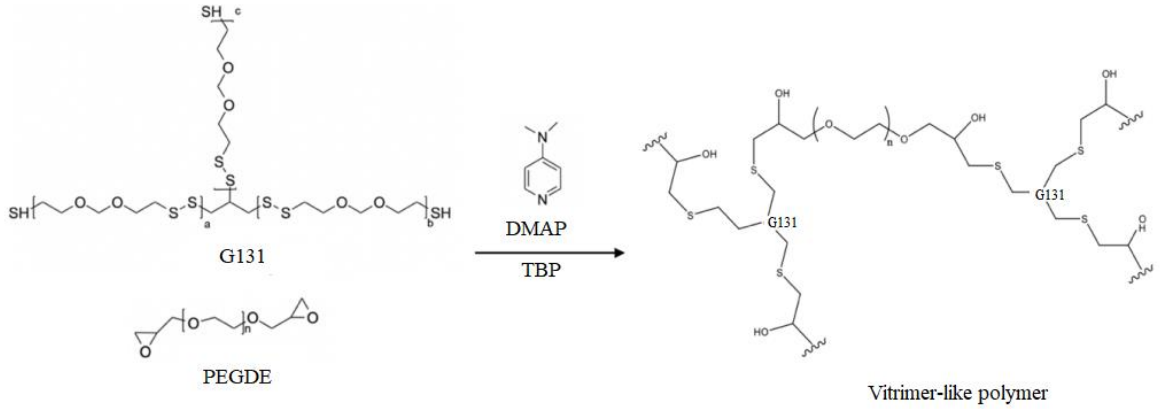

Figure 15: Crosslinking reaction of the thioplast G131 with PEGDE [36]

3.1.3. Reaction mechanism

The crosslinking reaction catalysed by DMAP can be separated in four main steps. In the first step, the initiation begins with the nucleophilic attack of DMAP to the epoxy ring, leading to the formation of a zwitterion. In the second step, a hydrogen exchange will rapidly lead to the formation of a hydroxy and a thiolate. That thiolate will attack the epoxy ring, in the third step, followed by the protonation of the alkoxide anion by a thiol group. Lastly, the thiolate addition on the cation will regenerate the DMAP and the reaction product (β-hydroxythioether) is obtained. This reaction can take place at room temperature but is accelerated at higher temperatures [37].

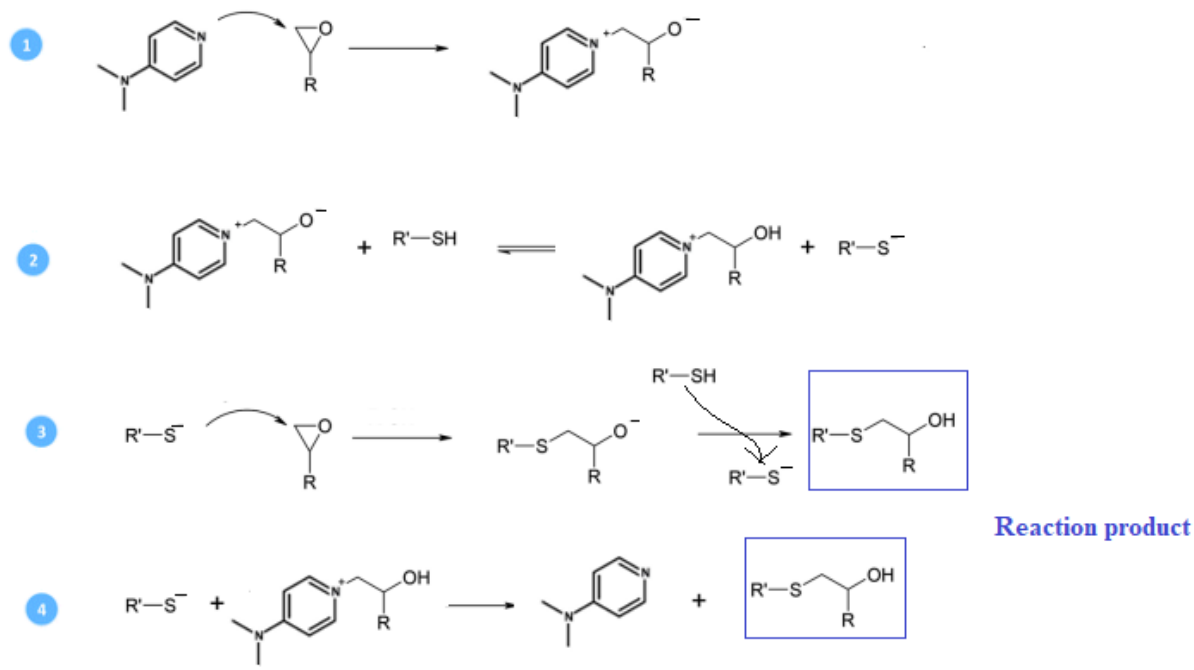

Figure 16: Crosslinking reaction mechanism [37]

3.2.Aim of this research

Now that you saw the chemical structure of the polymer network with a vitrimer behaviour, the aim of this research can be explained. The purpose of this work is to optimize the ionic conductivity and to assess the self-healing of this polymer network. The influence of two main parameters will be tested:

1) The molar mass of the crosslinker

The molar mass of the crosslinker will affect the tightness of the network and the movement of the polymer chains. A crosslinker with a low molar mass would give a tight network, hindering the movement of the chains, and thus diminishing the ionic conductivity. On the other hand, a higher ionic conductivity should be obtained with a high molar mass crosslinker as a lose network is formed. In such a network with high molar mass crosslinker, the number oxygen is also higher, promoting the transport of lithium ions through the coordination sites.

Therefore, to investigate the impact of the crosslinker molar mass on the ionic conductivity, polymer networks will be synthesized with PEGDE of 200, 500, 1100 and 2000 g/mol.

2) The crosslinking percentage

The crosslinking percentage can also affect the tightness of the network formed. With a lower crosslinking percentage, some thiol ends will not react, creating a loser network. The ionic conductivity and self-healing ability should be impacted positively by the diminution of the crosslinking percentage. Crosslinking percentages of 100% (fully crosslinked), 70%, 50% and 30% will be analysed on polymer networks with different molar mass of the crosslinker. The Figure 17 summarizes the polymer networks synthesized playing on the MW of the crosslinker as well as on the crosslinking percentage. As the PEGDE of 2000 g/mol is expensive, only networks with 30 and 70% of crosslinking were synthesized to test the ionic conductivity.

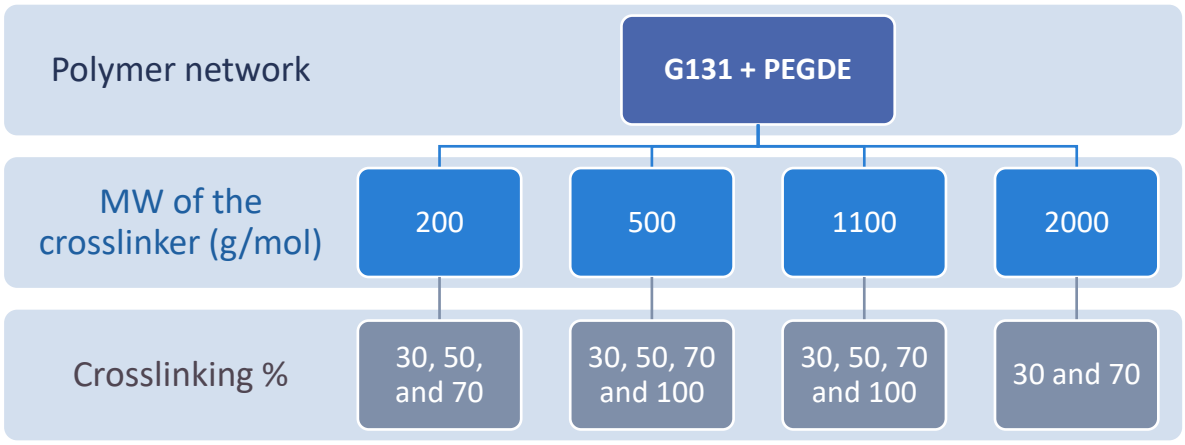

Figure 17: Polymer networks synthesized with different MW of the crosslinker and different crosslinking percentage

3.3. Plan of the experimental section and analysis

3.3.1. Network without lithium salt

The synthesis and characterization of the solid polymer electrolytes with a vitrimer behaviour can be separated into two main categories: the network with and without lithium salt. For the polymer network without lithium salt, the self-healing was assessed by tensile test and optical microscopy. Raman spectroscopy was performed to shed light on the disulfide bonds while a thermal characterization with DSC and TGA permitted to obtain the glass transition temperature and degradation temperature.

3.3.2. Network with lithium salt

A DSC was performed on the networks with lithium salt to compare with the ones without lithium salt. The electrochemical test (PEIS) was also performed on the polymer network with lithium salt.

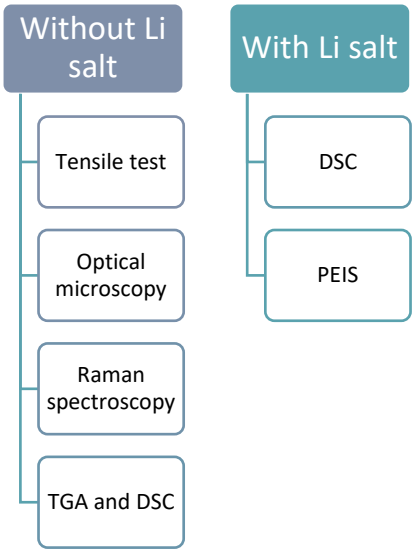

3.4. Reagents and chemicals

All reagents used are commercially available reagents.

Thioplast G131 was provided by Akzo Nobel (average MW = 5850 g/mol).

PEGDE was bought from Sigma Aldrich (MW=500 g/mol) and (MW=200 g/mol), while PEGDE (MW=1100 g/mol) and PEGDE (MW = 2000 g/mol) come from TCI.

The lithium salt $LiCLO_4$ (MW= 106,39, >95.0%), was supplied by Sigma Aldrich. The TBP (MW = 202,32 g/mol) was supplied by Sigma Aldrich as well. DMAP was bought from TCI (MW= 122,17 g/mol, >99.0%). Lastly, THF was purchased from VWR Chemicals BDH (MW=72,11 g/mol, T_B=66 ℃, d = 0,89 g/ml, >99%).

3.5. Methods

In this sub-section, the methods and parameters used for each analysis are described. A small explanation on each technique and the data obtained is also provided.

3.5.1. Raman Spectroscopy

Raman spectroscopy was performed to put in evidence the existence of the disulfide bonds for cross-linked samples after curing. The technique was executed on a Thermo-fisher Raman DXR coupled with Continuum microscope. The studied samples were subjected to 10 acquisitions with a laser of 532 nm wavelength through a 50 µm pinhole aperture.

3.5.2. Differential scanning calorimetry (DSC)

Differential scanning calorimetry (DSC) is a thermal analysis identifying phase transitions of a material. Phase transitions are measured by determining the difference in energy absorbed or released when the sample is cooled or heated compared to a reference. Examples of endothermic phase transition are glass transition and melting, whereas crystallization is an exothermic phase transition [38]. The DSC data is plotted in a graph with the heat flux transmitted to the sample as function of temperature. A typical DSC graph is shown in Figure 18.

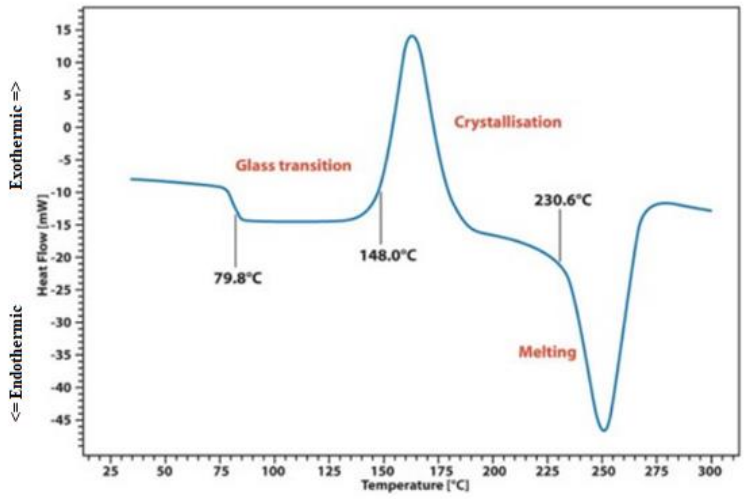

Figure 18: Typical DSC graph [39]

DSC measurements were carried out using a Mettler Toledo 822e calorimeter. Between 5 and 10 mg of product were analysed under nitrogen atmosphere with the flow of 50 mL/min in aluminum pan with an empty aluminum pan as reference cell. The samples were subjected to a first heating from -80 °C to 120 °C then cooled down to -80 °C and reheated up to 120°C

with a heating and cooling rate of 10 °C/min. Between each heating and cooling ramp, the temperature is maintained constant for 1 minute.

3.5.3. Thermo gravimetric analysis (TGA)

Thermogravimetric analysis (TGA) is a thermal analysis detecting the sample mass loss with the increase of the temperature. The thermal stability range and degradation temperature of a sample can be determined with this technique. TGA is performed using a microbalance placed in an oven under controlled atmosphere. A TGA graph represents the sample weight percentage as function of temperature (Figure 19). A compound is considered stable until reaching the temperature at which the mass loss of the compound is of 5%, That temperature corresponds to the degradation temperature (T_D 5%) [40].

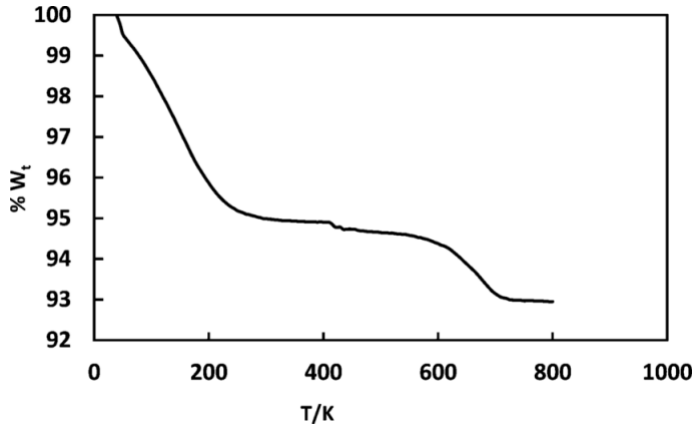

Figure 19: Typical TGA graph [41]

The TGA equipment used was a Mettler-Toledo TGA/SDTA 851e. The tests were performed under nitrogen atmosphere with the flow of 50 mL/min, in alumina crucibles with a volume of 70 µL. An empty alumina crucible was used as reference cell. The samples between 5 and 10 mg were subjected to heating from 25 °C to 500 °C with a heating rate of 10 °C/min.

3.5.4. Optical microscopy

Optical microscopy (OM) was performed in order to investigate self-healable properties of the dynamic network. The analysis was carried out on a AX70 microscope from Olympus coupled with an in-built HD camera.

3.5.5. Tensile testing

Tensile test was performed in order to assess the self-healing ability of the dynamic network. The analysis was carried out on a 6800 Series universal testing system from Instron. The speed of the elongation was of 10 mm/min and the sample dimensions are represented in Figure 20.

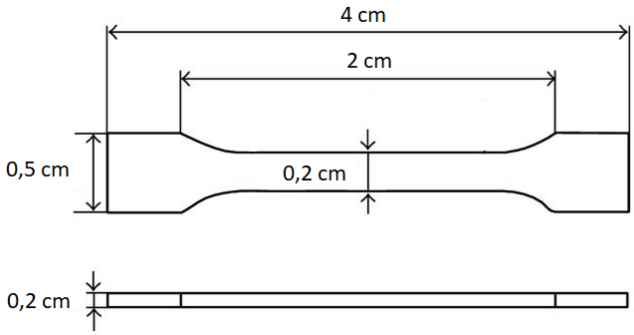

Figure 20: Tensile test, sample dimensions [42]

3.5.6. Potential electrochemical impedance spectroscopy (PEIS)

Potential electrochemical impedance spectroscopy (PEIS) measures the impedance of the sample. The resistance to the flow of an alternating current is called impedance. During a PEIS measurement, a small variation in potential is applied on the sample for different frequencies going from high frequency (MHz) to low frequency (mHz or µHz). The impedance can be calculated with the following formula:

Equation 2: Impedance formula

$$U = Z * I$$

Where Z is the impedance, I the current (in A), and U is the potential applied (in V). The intrinsic conductivity of the sample can be easily deduced knowing the impedance and dimensions of that sample.

Equation 3: Relationship impedance and intrinsic conductivity

$$Z = \frac{1}{\sigma} * \frac{l}{A}$$

Where σ (in S) is the intrinsic conductivity, l (in cm) is the thickness of the sample, and A (in cm^2) is the electrode contact area. The Nyquist diagram represents the impedance response with the imaginary impedance as function of the real impedance. The overall impedance (in Ohm) is given by the red dot in Figure 21. The ionic conductivity of the sample can be deduced with the overall impedance [43], [44], [45] .

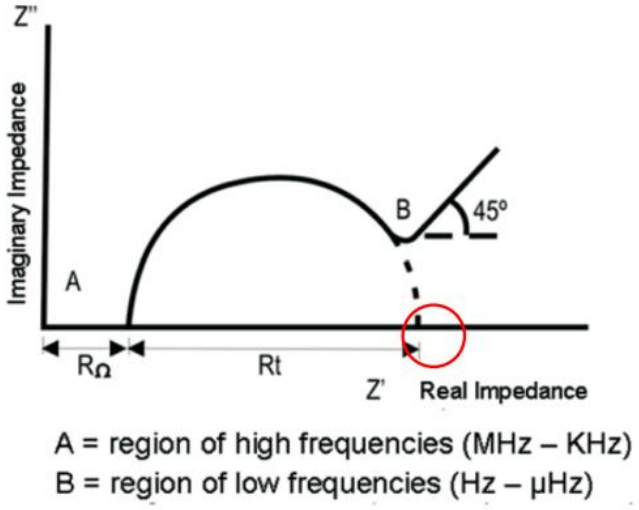

Figure 21: Typical representation of a Nyquist diagram [46]

PEIS measurements were performed using a VMP-300 Potentiostat 48 apparatus from BioLogic over a frequency range of 7 MHz to 100 mHz and with an amplitude AC excitation voltage of 10 mV. The electrochemical cells were placed into the temperature chamber. Thus, the electrochemical impedance spectra were collected for a temperature range from 60 °C to 20 °C by gradually decreasing the temperature by steps of 10 °C with an equilibration time of 1h between each measurement. The thickness of the sample (2 stainless steel disks + electrolyte) was measured with a micrometer after opening the coin cell. The thickness of the electrolyte is then deduced, knowing the thickness of the stainless steel disks.

3.6. Experimental protocol

3.6.1. Polymer network without lithium

The weight of the different reagents will depend on the initial weight of G131 as well as the crosslinking percentage. To obtain a fully crosslinked network, the ratio n_{SH}/n_{epoxy} is equal to 2/3. This ratio is multiplied by the crosslinking percentage wanted to obtain a polymer network with 30, 50 or 70% crosslinking.

Table 2: Weight of the reagents to prepare the polymer network

Reagents	Theoretical weight
PEGDE	$m_{PEGDE} = \frac{3}{2} * \frac{\alpha * m_{G131}}{M_{G131}} * M_{PEGDE}$ Where α is the crosslinking percentage while the ratio 3/2 corresponds to the number of functional groups on G131 and PEGDE respectively.
DMAP	$m_{DMAP} = \frac{m_{G131} + m_{PEGDE}}{100}$ 1 wt% of DMAP is used
TBP	$m_{TBP} = 0{,}3 * \frac{m_{G131} + m_{PEGDE} + m_{DMAP}}{100}$ 0,3 wt% of TBP is used

One gram of thioplast G131 is introduced in a 10 mL glass vial. DMAP (0,1 wt%) is grinded and poured in the vial with the thioplast G131. PEGDE with a low molecular weight (MW = 200 g/mol and 500 g/mol) is added directly to the vial while PEGDE with a high molecular weight (MW = 1100 g/mol and 2000 g/mol) is placed in a separate vial and dissolved in 1 mL THF, then transferred in the vial with the thioplast. TBP (0,3 wt%) is added with a micropipette to the vial. The mixture is stirred manually with a spatula until it becomes homogeneous. After that, the vial is placed in the vacuum oven for 48 hours at room temperature to remove bubbles trapped in the mixture. The last step consists in curing the network for 5 hours at 60 °C in the oven under vacuum.

A network with G131 and PEGDE 500 g/mol obtained after the cure is shown in Figure 22.

Figure 22: Aspect of the cured network of thioplast G131 + PEGDE 500 g/mol

3.6.2. Tensile test, sample preparation

Tensile samples were prepared with networks of thioplast G131 with PEGDE 500 g/mol containing different crosslinking percentages. The first steps are identical to the formation of the polymer network, except for the quantity of thioplast G131 which is of 4 grams instead of 1 gram. However, the mixture is not placed under vacuum, but is poured in a Teflon mould with a dog-bone shaped form. As the vacuum oven would remove bubbles too quickly, resulting to an inhomogeneous surface of the sample, the samples stay under the hood for 48 hours to gently remove the bubbles. If bubbles still appear, they are popped with a needle. Lastly, the samples are cured for 5 hours at 60 °C in the oven. Tensile test samples crosslinked at 70% and 30% are shown in Figure 23.

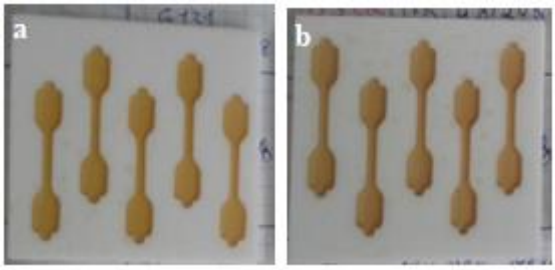

Figure 23: Tensile test samples with G131 + PEGDE 500 g/mol crosslinked at 70% (a) and 30% (b)

To test them, the samples are marked at 2 centimetres distance (where the grips will hold the sample) and in the middle of the sample. One of the samples is directly tested as reference whereas the other samples are cut in two then tested after 2, 4, 6 and 24 hours. This test was repeated three times for each sample and the average curve of those three tests is represented in the section 4.3.2.

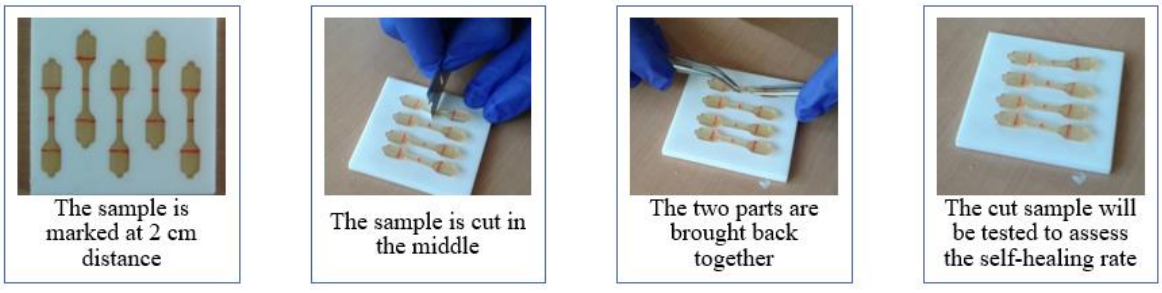

Figure 24: Tensile sample preparation before testing

3.7. Electrolyte formation

3.7.1. Film formation

The lithium salt ($LiClO_4$) is added into the network for electrochemical tests. For this preparation, the first steps are similar to the film formation without lithium, but the polymer network is only placed for 24 hours in the oven under vacuum at room temperature. Then, 300 mg of the uncured network are placed in a glass vial and dissolved in 0,5 mL THF. The amount of lithium salt ($LiClO_4$) is calculated and weighted in another vial. The lithium salt is dissolved with 0,3 to 0,5 mL of THF.

Table 3: Weight of $LiClO_4$ needed in the polymer network

Percentage of $LiClO_4$	**Theoretical weight**
10 wt%	$m_{\mathrm{LiClO4}} = \frac{10 * m_{uncured\ polymer\ network}}{90}$ For 300 mg of polymer network, 33,33 mg of lithium salt are needed to attain 10 wt%.
20 wt%	$m_{\mathrm{LiClO4}} = \frac{20 * m_{uncured\ polymer\ network}}{80}$ For 300 mg of polymer network, 75 mg of lithium salt are needed to attain 20 wt%.
30 wt%	$m_{\mathrm{LiClO4}} = \frac{30 * m_{uncured\ polymer\ network}}{70}$ For 300 mg of polymer network, 128,57 mg of lithium salt are needed to attain 30 wt%.

Both the vial with the polymer network and the lithium salt are stirred overnight on the magnetic stirrer. After that, the lithium salt solution is transferred into the polymer vial (Li vial is rinsed with 2 times 0,1 mL of THF). This mixture of polymer network + lithium salt is stirred 48 hours on the magnetic stirrer to obtain a homogeneous solution. Then, the whole mixture (concentration ~0,3g/mL) is poured into a 4 cm diameter Teflon mould. The THF is evaporated for two nights before curing the polymer network with lithium salt for 5 hours at 60°C in the oven under vacuum. After curing, the film can be removed from the mould and cut down in small disks for electrochemical tests as shown in Figure 25 and Figure 26. The

film obtained is self-standing as shown in Figure 26 and possesses a thickness around 100 µm.

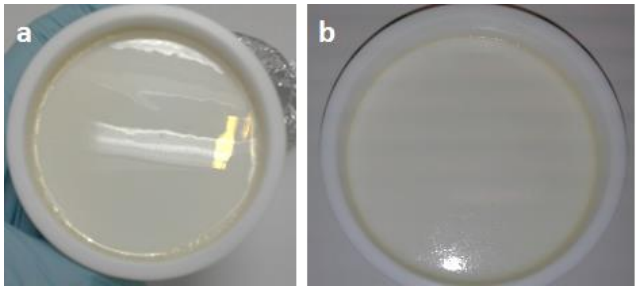

Figure 25: Network with lithium before curing (a) and after curing (b)

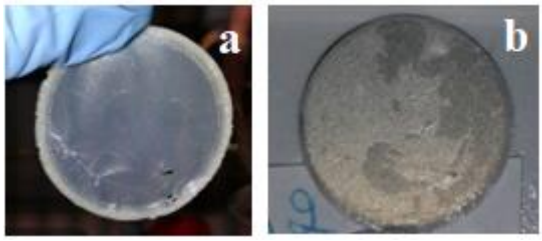

Figure 26: Self-standing SPE film (a), and SPE on stainless steel (b)

Drop casting was a method previously used for the film formation. But that method was replaced by the Teflon moulds since the films produced contained too many bubbles. The exact experimental protocol of the drop casting is described in Appendix A – Film formation by dropcasting.

3.7.2. PEIS cell formation

Once the SPE has been synthesized, a coin cell with that SPE can be prepared for electrochemical tests. All the coin cells are formed and closed in an argon glovebox (under inert atmosphere). For PEIS, the SPE is placed between two stainless steels disks as described in Figure 27.

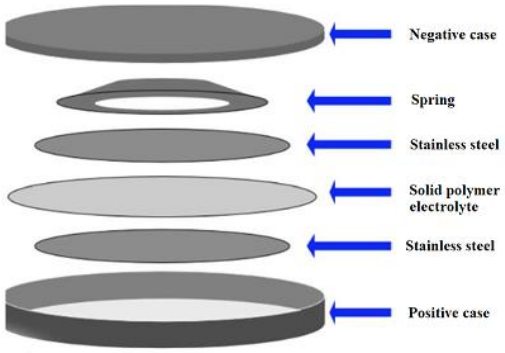

Figure 27: Coin cell for PEIS measurements [47]

4. Results and discussion

In the previous section, the preparation of a solid polymer electrolyte with a vitrimer behaviour was detailed. That SPE is a polymer network based on thioplast G131 and crosslinked by PEGDE. The polymer network without lithium salt was analysed by Raman spectroscopy as well as DSC and TGA to obtain a structural and thermal characterization. Moreover, the self-healing ability of the polymer network without lithium salt was assessed by optical microscopy and tensile test. On the polymer network with lithium salt (thus the SPE), DSC and PEIS were performed. In this section, the results obtained will be shown and discussed with a particular attention to PEIS, as the aim of this work is to optimize the ionic conductivity of this SPE.

4.1.Structure characterization of the solid polymer electrolyte

4.1.1. Raman Spectroscopy

Disulfide bonds in the polymer network are essential to attain a vitrimer-like behaviour. Raman spectroscopy was carried out to put in evidence the S-S and C-S bonds. Spectra of crosslinked G131 with PEGDE 200, 500 and 1100 g/mol are presented in Graph 1. The Raman intensity is plotted as function of the Raman shift (in cm^{-1}). The crosslinked network should show peaks of S-S stretching vibrations (430-550 cm^{-1}), C-S stretching vibrations (630 – 790 cm^{-1}), CH_2 stretching vibrations (2900-2940 cm^{-1} and 1400 – 1450 cm^{-1}), the ether bond C-O-C (800-950 cm^{-1}), S-H stretching vibration (2550-2600 cm^{-1}) [48]. All those peaks were annotated on the Graph 1. Based on the presence of C-S and S-S peaks in the networks with different PEGDE, it can be concluded that the disulfide bond was conserved during the chemical reaction and thermal curing. A vitrimer-like behaviour should thus be observed in the samples studied. No thiol peak (2550-2600 cm^{-1}) was detected which is coherent because investigated the samples are 100% crosslinked, meaning that all the thiols should have reacted.

The Raman spectra of the polymer networks with different MW of PEGDE are quite identical, except for the intensity of the CH_2 peaks. The intensity of this peak is the highest for the network with PEGDE 1100 g/mol, and the lowest with PEGDE 200 g/mol. This is coherent as the PEGDE 1100 possesses the longest polymer backbone and thus more CH_2.

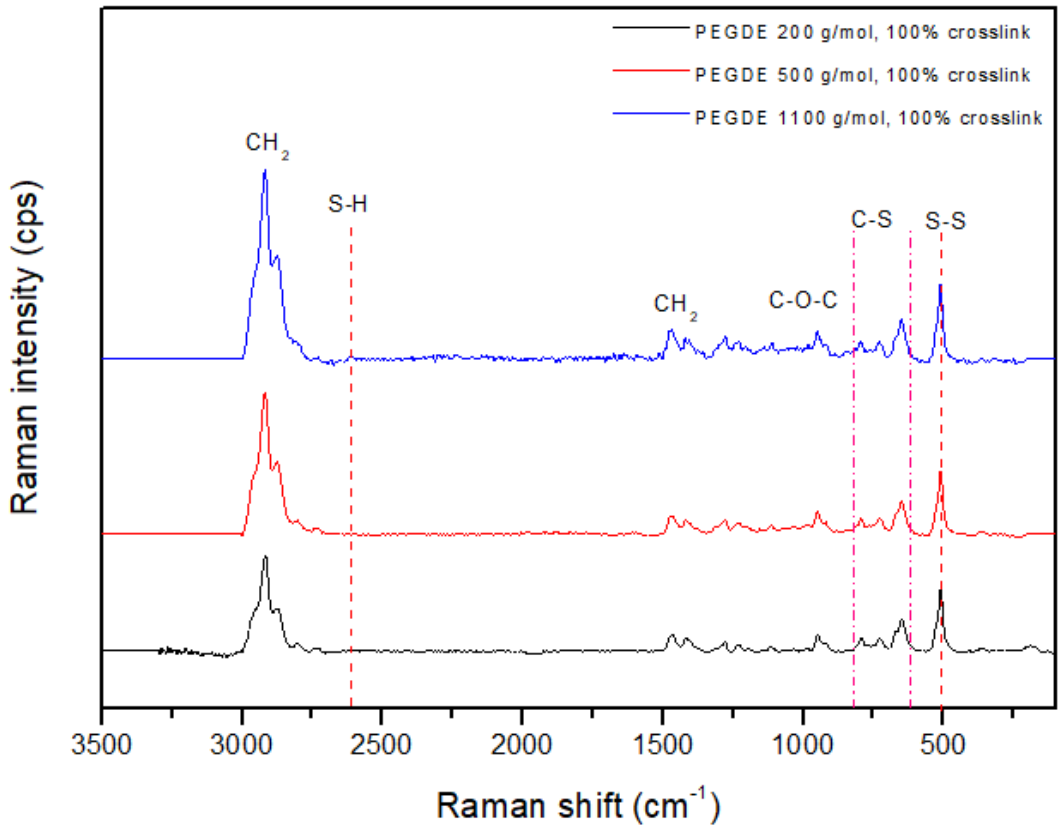

Graph 1: Raman spectra of the 100% crosslinked G131 with PEGDE 200 g/mol, 500 g/mol, and 1100 g/mol.

4.2.Thermal characterization of the solid polymer electrolyte

4.2.1. Differential scanning calorimetry (DSC)

The T_g of the examined SPEs has been determined using DSC (Table 4, Table 5 and Table 6). This temperature is crucial in the context of SPEs since it should result in a higher ionic conductivity above T_g due to a better segmental mobility. Firstly, the influence of the molecular weight of the PEGDE on the T_g was analysed. After that, the effect of the crosslinking percentage on the T_g was evaluated. Lastly, the impact of the addition of lithium salt on the T_g was observed.

4.2.1.1. Influence of the MW of PEGDE

DSC heating curves for the crosslinked G131 with PEGDE 200, 500, and 1100 g/mol before the addition of $LiClO_4$ (and crosslinked at 100%) are represented in Graph 2. Those three polymer networks undergo one transition from glassy to rubbery state around -53 °C. No melting and crystallization transitions were observed for the networks with PEGDE 200,

500, and 1100 g/mol, indicating the amorphous nature of the polymer networks (see Appendix B – DSC graphs).

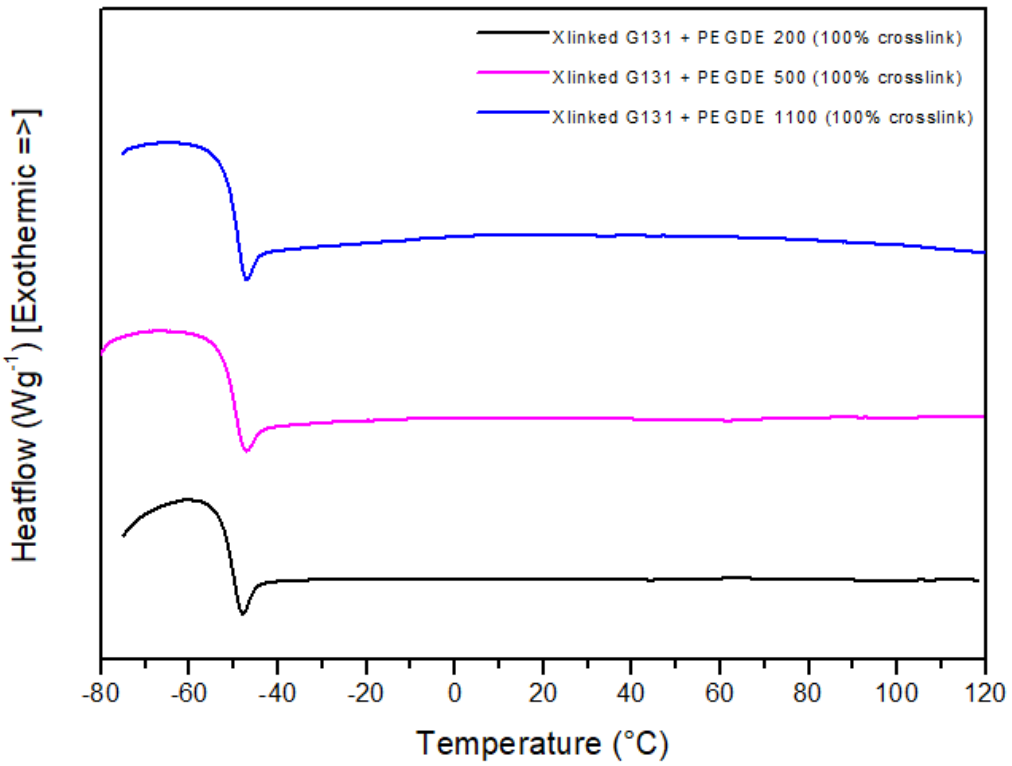

Graph 2: DSC heating curves of the 100% crosslinked G131 with PEGDE 200 g/mol, 500 g/mol, and 1100 g/mol

The T_g values obtained with different molecular weights of PEGDE are reported in Table 4.

Table 4: T_g values of the 100% crosslinked polymer network with different MW of PEGDE

Sample	Glass transition temperature (°C)
Xlinked G131 + PEGDE 200 g/mol, crosslinked at 100%	-53
Xlinked G131 + PEGDE 500 g/mol, crosslinked at 100%	-53
Xlinked G131 + PEGDE 1100 g/mol, crosslinked at 100%	-52

4.2.1.2. Influence of the crosslinking percentage

DSC heating curves for the crosslinked G131 with PEGDE 500 g/mol containing 30, 50, 70 and 100% crosslinking (before the addition of $LiClO_4$) are shown in Graph 3. When decreasing the crosslinking density, the T_g is barely influenced. As we can see in Table 5, an average T_g of -51 °C is observed for the crosslinked G131 with PEGDE 500 g/mol at different crosslinking percentages.

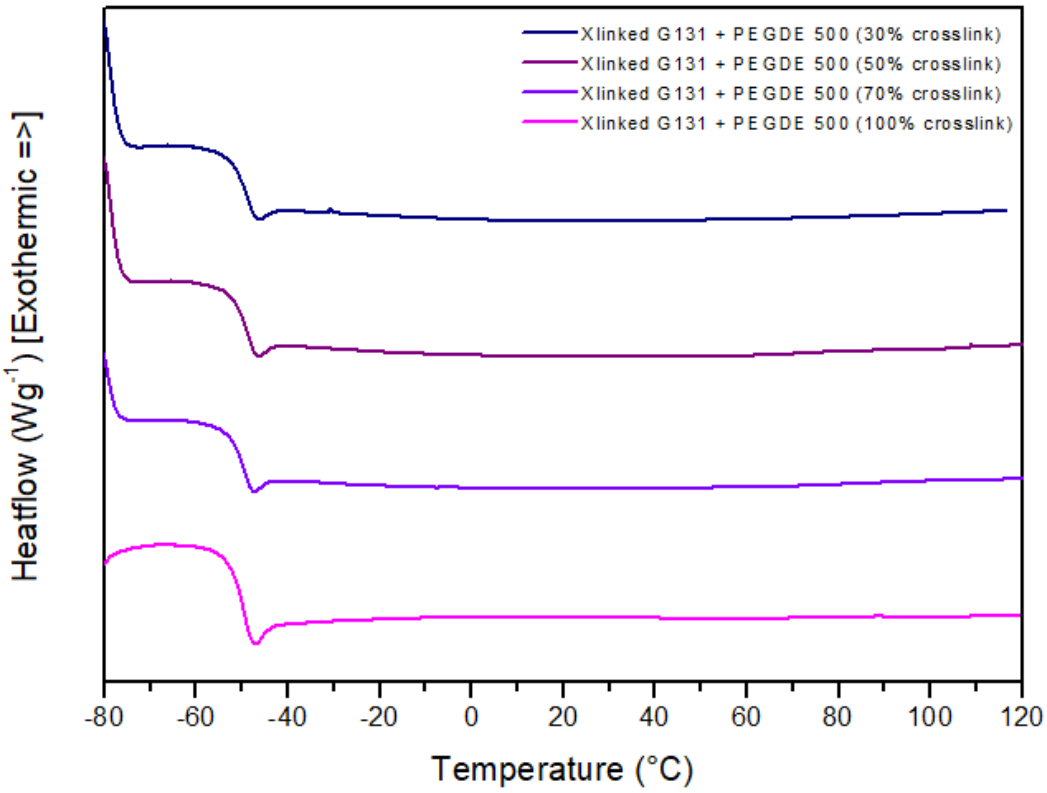

Graph 3: DSC heating curves of the 30, 50, 70 and 100% crosslinked G131 with PEGDE 500 g/mol

The T_g values obtained with different crosslinking percentages are shown in Table 5.

Table 5: T_g values of the 30, 50, 70 and 100% crosslinked G131 with PEGDE 500 g/mol

Sample	Glass transition temperature (°C)
Xlinked G131 + PEGDE 500 g/mol, crosslinked at 30%	-50
Xlinked G131 + PEGDE 500 g/mol, crosslinked at 50%	-50
Xlinked G131 + PEGDE 500 g/mol, crosslinked at 70%	-51
Xlinked G131 + PEGDE 500 g/mol, crosslinked at 100%	-53

4.2.1.3. Influence of the $LiClO_4$

DSC heating curves for the crosslinked G131 with PEGDE 500 g/mol (100% crosslinked) with 0, 10, and 20 wt% of $LiClO_4$ are shown in Graph 4. The addition of Li salt increased the T_g, confirming the interaction of $LiClO_4$ with the polymer as usually observed for PEO-based SPEs [49]. The crosslinked G131 with PEGDE 500 g/mol (100% crosslinked) shows a glass transition temperature of -53 °C without $LiClO_4$, while that value drops to -35 °C for 10 % and 20 % of added lithium. But the amount of $LiClO_4$ added itself does not affect the T_g significantly.

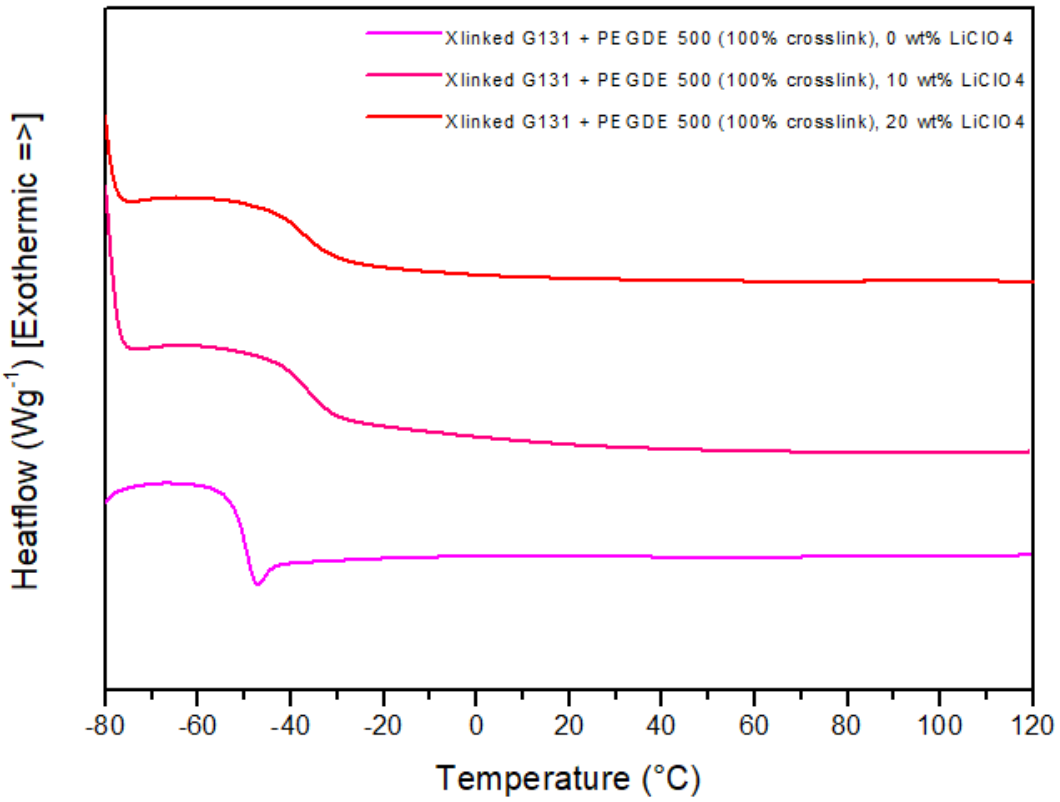

Graph 4: DSC heating curves of the 100% crosslinked G131 with PEGDE 500 g/mol with 0, 10 and 20 wt% of $LiClO_4$

The T_g values obtained with different weight percentages of $LiClO_4$ are reported in Table 6.

Table 6: T_g values of the 100% crosslinked G131 with PEGDE 500 g/mol, with 0, 10 and 20 wt% in $LiClO_4$

Sample	**Glass transition temperature (°C)**
Xlinked G131 + PEGDE 500 g/mol, crosslinked at 100%, 0 wt% $LiClO_4$	-53
Xlinked G131 + PEGDE 500 g/mol, crosslinked at 100%, 10 wt% $LiClO_4$	-35
Xlinked G131 + PEGDE 500 g/mol, crosslinked at 100%, 20 wt% $LiClO_4$	-35

We can therefore draw the conclusion that in our system, the addition of $LiClO_4$ rather than the crosslinking density has a greater impact on the T_g.

4.2.2. Thermo gravimetric analysis (TGA)

The thermal stability of the investigated polymers has been evaluated using TGA. By deriving weight loss as a function of temperature, the thermal stability is defined as the

temperature at which the sample experiences a maximum rate of weight loss. The results are shown in Graph 5, where the weight loss is expressed in function of the temperature.

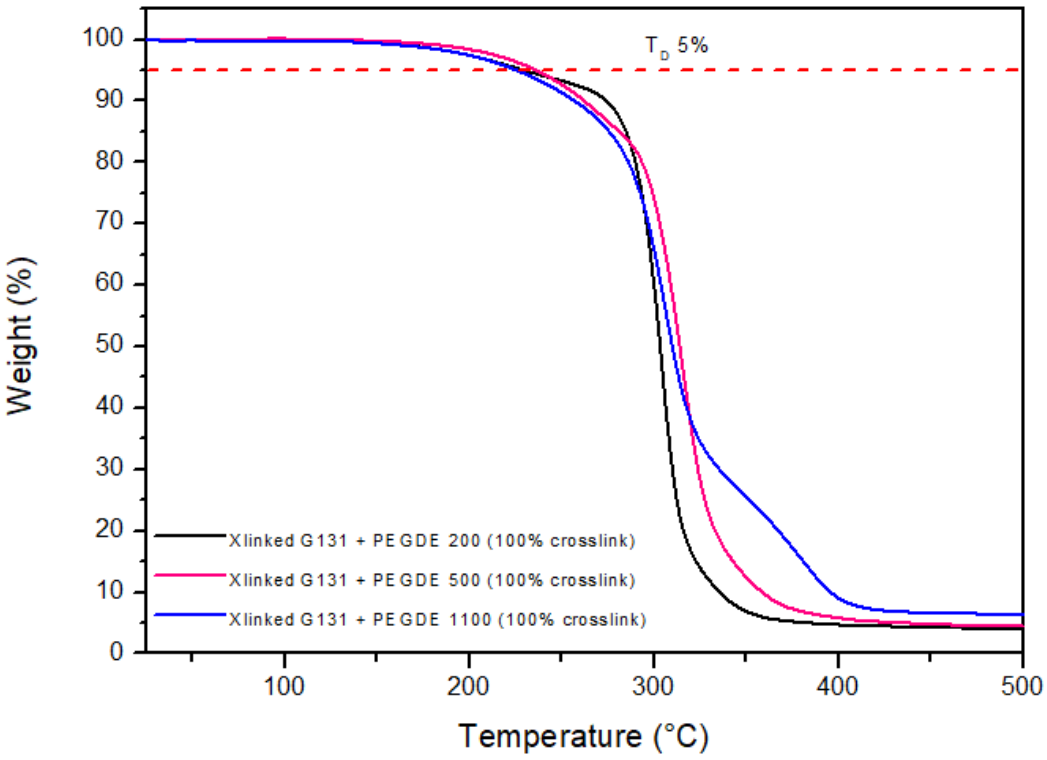

Graph 5: TGA curves of the 100% crosslinked G131 with PEGDE 200 g/mol, 500 g/mol and 1100 g/mol.

In this graph, the degradation temperature (T_D 5%), corresponding to a 5 % weight loss, can be seen and the values are reported in Table 7. The average degradation temperature of the three polymer networks is of 230°C.

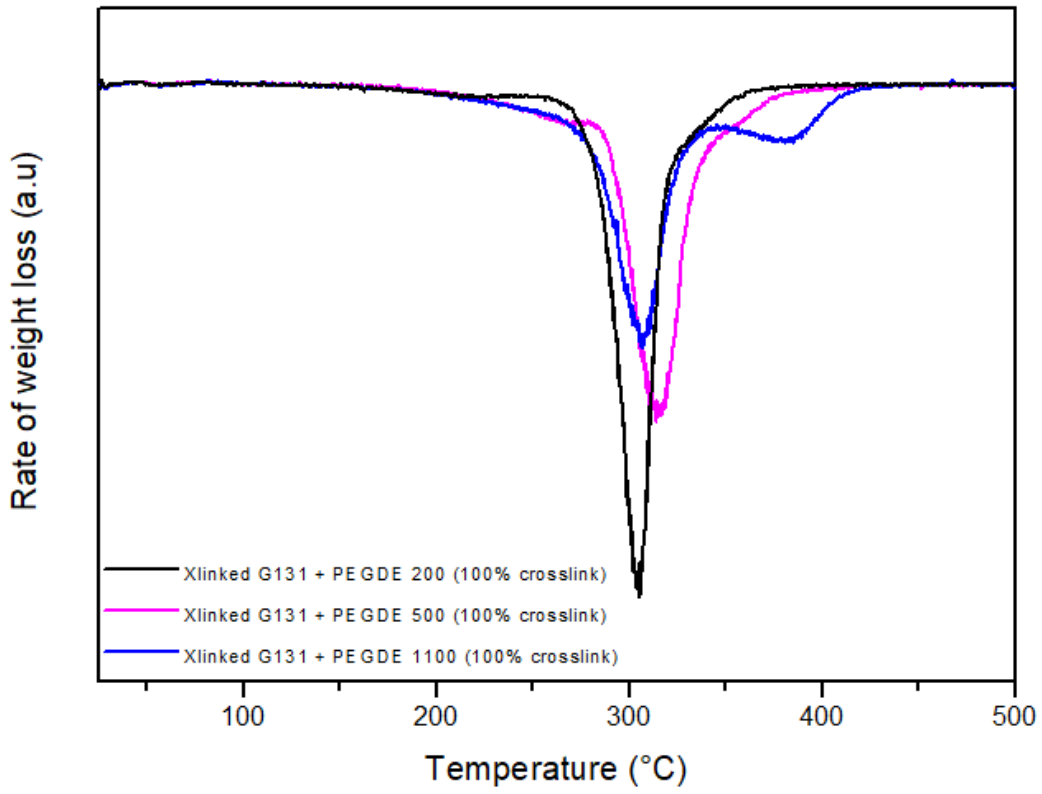

Graph 6: TGA first derivative curves of the 100% crosslinked G131 with PEGDE 200 g/mol, 500 g/mol, and 1100 g/mol.

The first derivative of the TGA curves is represented in Graph 6. The maximum rate loss is observed around 310 °C for the three polymer networks. However, the crosslinked G131 with PEGDE 1099 (100% crosslink) shows two peaks, the majority of the polymer network degrades at 310 °C while the rest is degraded at 380 °C.

Table 7: TGA degradation temperature and thermal stability of the polymer networks

Sample	**T_D 5% (°C)**	**Temperature at maximum rate loss (°C)**
Xlinked G131 + PEGDE 174 g/mol	229	302
Xlinked G131 + PEGDE 500 g/mol	236	315
Xlinked G131 + PEGDE 1099 g/mol	225	307

The lack of significant differences between samples can be attributed to the fact that all of the polymers under investigation have the same polysulfide backbone. In order to conclude this section, it should be noted that the thermal stability of the investigated polymer systems is consistently high enough for further usage as SPEs in batteries.

4.3. Self-healing performances of the solid polymer electrolyte

4.3.1. Optical microscopy

The self-healing behaviour of the crosslinked G131 with PEGDE 500 g/mol was assessed by optical microscopy, for the networks crosslinked at 100, 70, 50 and 30%. After 24 hours, the width of the cut is measured to observe the self-healing of the sample. The optical microscopy measurement of the crosslinked G131 with PEGDE 1100 g/mol is presented in Appendix C – Optical microscopy.

4.3.1.1. Crosslinked G131 with PEGDE 500 g/mol (100% crosslink)

For the network crosslinked at 100%, the width of the cut performed on the sample barely changed after 24 hours. The images and width of the cut after 0 and 24 hours are reported in Table 8.

Table 8: Optical images of the network crosslinked at 100%

After 0 hours	**After 24 hours**
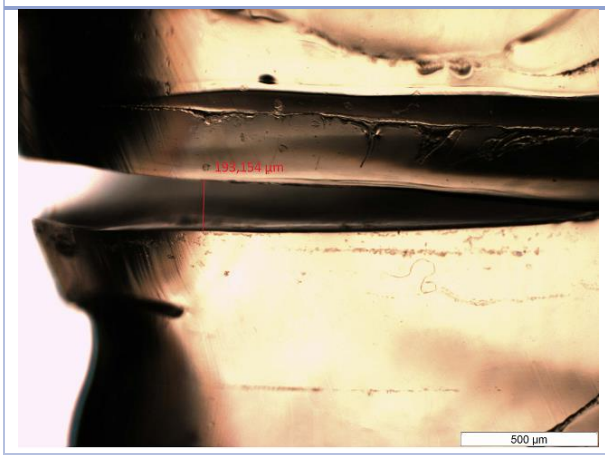	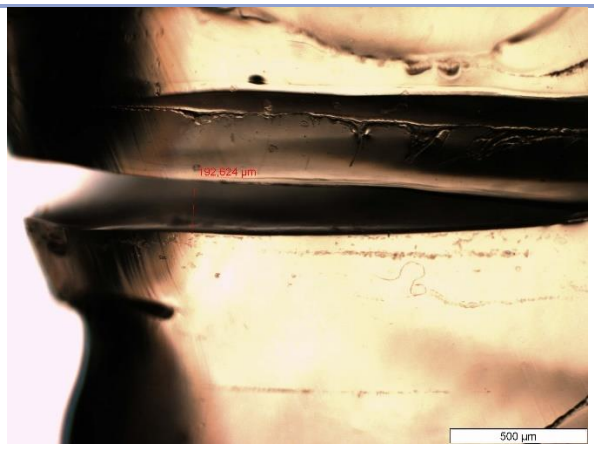
Distance: 193 µm	**Distance:** 193 µm

4.3.1.2. Crosslinked G131 with PEGDE 500 g/mol (70% crosslink)

For the network crosslinked at 70%, the width of the cut performed on the sample became larger after 24 hours. The images and width of the cut after 0 and 24 hours are reported in Table 9. However, the length of the cut itself became slightly smaller, showing that the self-healing occurs but quite slowly.

Table 9: Optical images of the network crosslinked at 70%

After 0 hour	**After 24 hours**

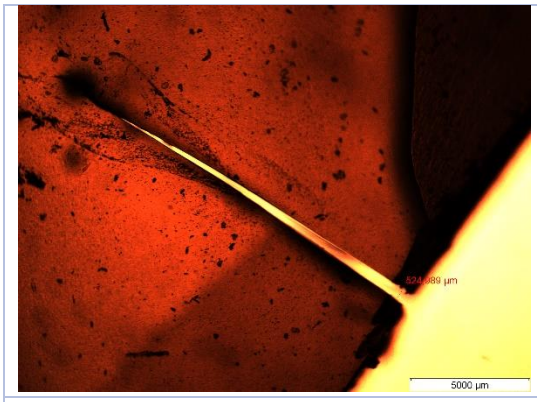	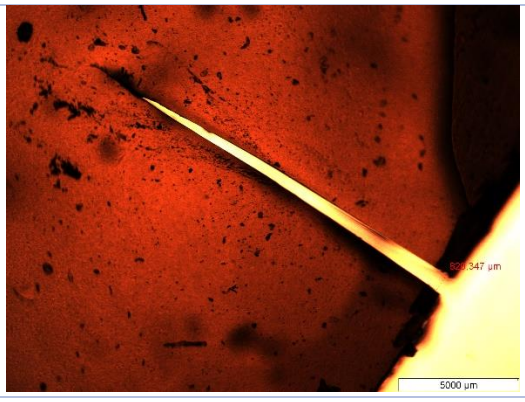
Distance: 525 µm	**Distance:** 820 µm

4.3.1.3. Crosslinked G131 with PEGDE 500 g/mol (50% crosslink)

For the network crosslinked at 50%, the width of the cut performed on the sample became a bit smaller after 24 hours. The images and width of the cut after 0 and 24 hours are reported in Table 10.

Table 10: Optical images of the network crosslinked at 50%

After 0 hour	After 24 hours
	
Distance: 3 885 µm	**Distance:** 3 617 µm

4.3.1.4. Crosslinked G131 with PEGDE 500 g/mol (30% crosslink)

For the network crosslinked at 30%, the width of the cut performed on the sample got somewhat smaller after 24 hours. The images and width of the cut after 0 and 24 hours are reported in Table 11.

Table 11: Optical images of the network crosslinked at 30%

After 0 hours	After 24 hours

	
Distance: 1 926 µm	**Distance:** 1 832 µm

4.3.2. Tensile test

Tensile testing was performed to demonstrate the crosslinked samples self-healing percentage at room temperature after achieving a certain degree of self-healing with a crosslinking percentage lower than 100%. Therefore, the crosslinked samples at 70 and 30 % were tested.[1] Five specimens were prepared and tested following the protocol explained in section 3.6.2, Figure 24.

4.3.2.1. Crosslinked G131 with PEGDE 500 g/mol (30% crosslinking)

The behaviour of a vitrimer-like material under tension can be clearly seen in the tensile test graph. The applied force (in Newton) is plotted against the specimen's proportional displacement (%).

The measurement began by stretching the first specimen, not cut which is considered as a reference point for the self-healing ability percentage. In Graph 7, a flat line at zero force is depicted at the start of the test for the not cut sample (t = 0 hrs), as no load is being applied to the specimen at that time. The testing process started with a not-cut sample, which we used as a benchmark for the self-healing ability percentage.

The 30% crosslinked G131 network then experiences elastic deformation in the elastic zone as the deformation is gradually applied. The graph appearance demonstrates that the network reached 335 % as displacement at the break, with a sudden drop in force and without substantial elongation; meaning that the sample is brittle.

[1] The 50% crosslinked network could not be tested due to an operating malfunction

After testing the reference sample, we cut the 4 remaining specimens in the middle them brought them back together at the same time and left them to self-heal. The second specimen tested was the one self-healed for 4 hours, the third one after 6 hours and the last one after 24 hours. We observe in the graph, an increase in the self-healing percentage from 30 % to 78 % by just 4 hours of difference. The self-healing % was calculated according to Equation 4:

Equation 4: Self-healing percentage

$$self - healing\ (\%) = \frac{displacement\ at\ break\ at\ t_i}{displacement\ at\ break\ at\ t_0} \cdot 100$$

For the last specimen, tested after 24 hours from bringing the two parts together didn't self-heal for more than 37 %. This could be due to the fact that some S-S bonds can undergo oxidation when exposed to oxygen (O_2) and that they are self-healing faster within the same cut part.

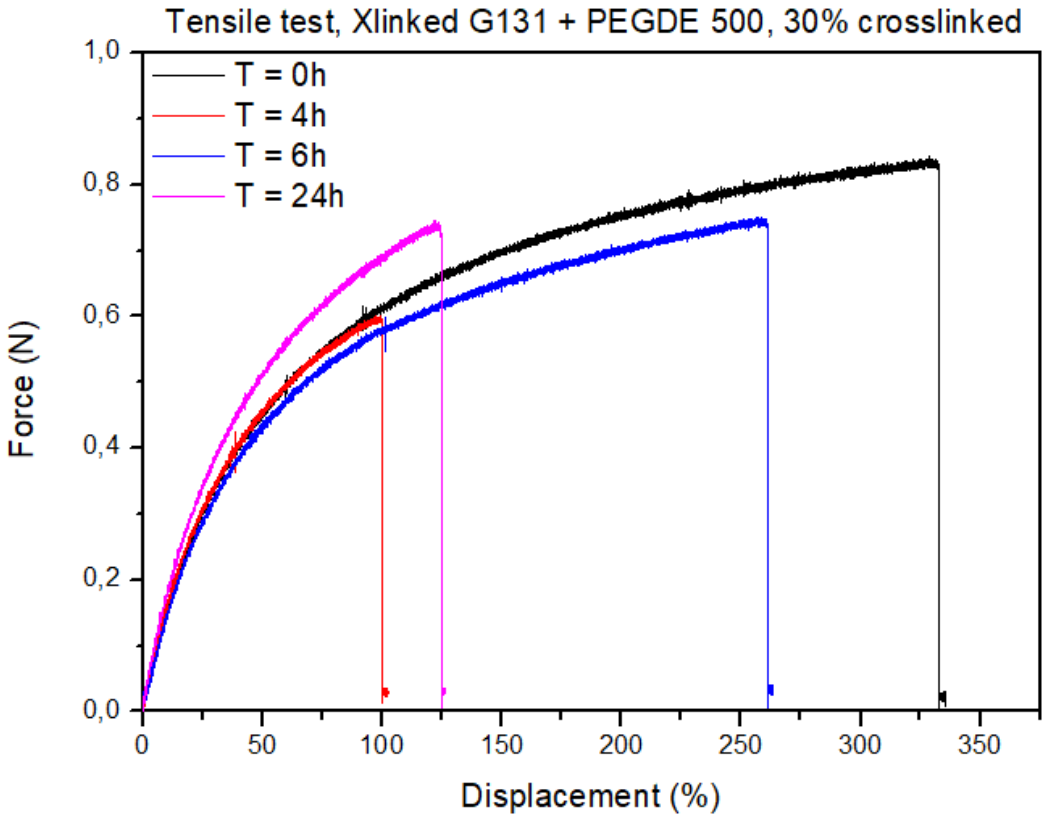

Graph 7: Tensile test of the crosslinked G131 with PEGDE 500 g/mol (30% crosslink) after 0 (not cut), 4, 6, and 24 hours (cut)

The tensile test values such as the displacement at break and the self-healing are reported in Table 12.

Table 12: Tensile test values of the 30% crosslinked G131 network

Time	Displacement at break (%)	Modulus (MPa)	Self-healing (%)	Force at break (N)	Maximum force (N)
0h	335	0,44	/	0,83	0,83
4h	100	0,44	30	0,60	0,60
6h	261	0,21	78	0,74	0,74
24h	125	0,56	37	0,73	0,73

4.3.2.2. Crosslinked G131 with PEGDE 500 g/mol (70% crosslinking)

Same as for the 30 % crosslinked G131, the one crosslinked at 70 % showed similar results (Graph 8). The displacement at break is 511 %, 113 %, 139 %, 186 % and 163 % for samples measured at t = 0, 2, 4, 6, and 24 hours respectively. These samples showed a self-healing percentage of 22, 27, 36, and 32 % respectively.

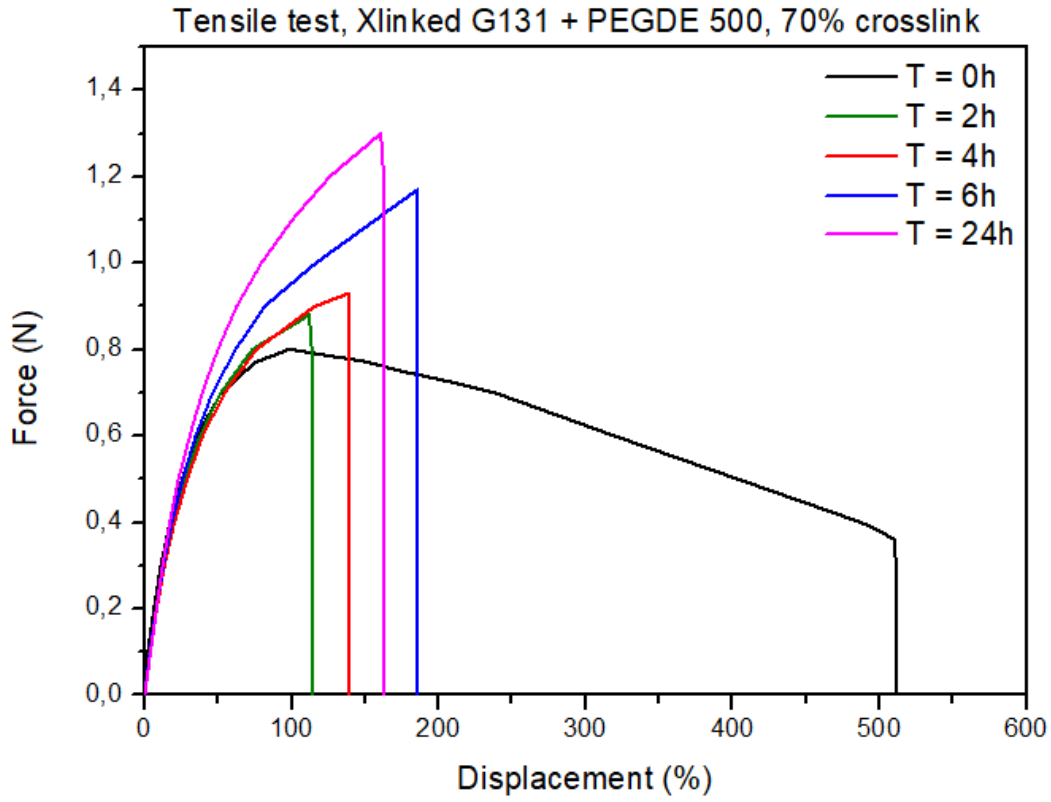

Graph 8: Tensile test of the crosslinked G131 with PEGDE 500 g/mol (70% crosslink) after 0 (not cut), 4, 6, and 24 hours (cut)

The tensile test values such as the displacement at break and the self-healing are reported in Table 13.

Table 13: Tensile test values of the 30% crosslinked G131 network

Time	Displacement at break (%)	Modulus (MPa)	Self-healing (%)	Force at break (N)	Maximum force (N)
T = 0h	511	0,76	/	0,38	0,8
T = 2h	114	0,51	22	0,88	0,88
T = 4h	139	0,54	27	0,93	0,93
T = 6h	186	0,70	36	1,17	1,17
T = 24h	163	0,65	32	1,3	1,3

The self-healing of the networks crosslinked at 30% and at 70% were compared in Graph 9. For all the measurement times, the self-healing is better for the network crosslinked at 30% than the one at 70%. This can be explained by the fact that decreasing the crosslinking density will give more mobility to the polymer chains, thus facilitating the disulfide metathesis as the chains can come close to each other more easily.

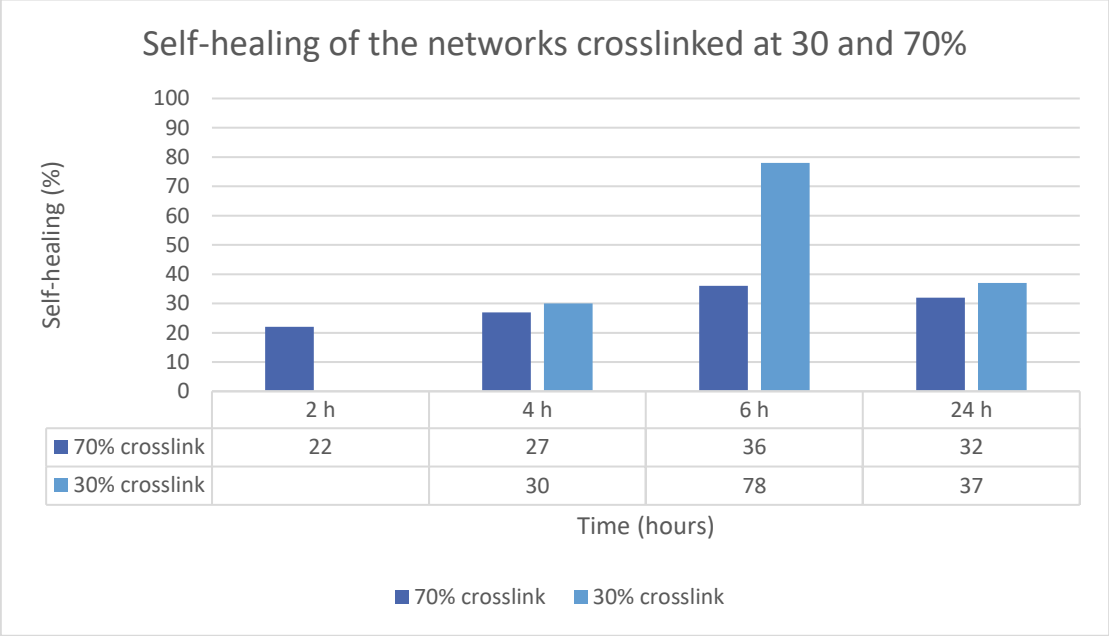

Graph 9: Comparison of the self-healing between the network crosslinked at 30 and 50%

4.4. Electrochemical characterization of the solid polymer electrolyte

4.4.1. Potential electrochemical impedance spectroscopy (PEIS)

To study the effect of the crosslinking percentage and MW of the PEGDE on the ionic conductivity, different SPEs were prepared. The following points are detailing the networks with PEGDE of 200, 500, 1100 and 2000 g/mol. For each MW of PEGDE, different crosslinking percentages were tested with 10 or 20 wt % of $LiClO_4$. All the SPEs were prepared as described in the point 3.7.

The ionic conductivity was measured from 20 °C to 60 °C to observe the increase of ionic conductivity at higher temperature. The ionic conductivity was determined from the resistance (R in Ω) extracted from the Nyquist diagram (see point 3.5.6). Knowing the area (A in cm^2) and thickness (l in cm) of the electrolyte, the ionic conductivity (in S/cm) was calculated with the following formula:

Equation 5: Ionic conductivity

$$\sigma = \frac{l}{R * A}$$

4.4.1.1. Network with PEGDE 200 g/mol

The logarithm of the ionic conductivity (in S/cm) was plotted as function of 1000/temperature (in K^{-1}), and the results are represented in Graph 10.

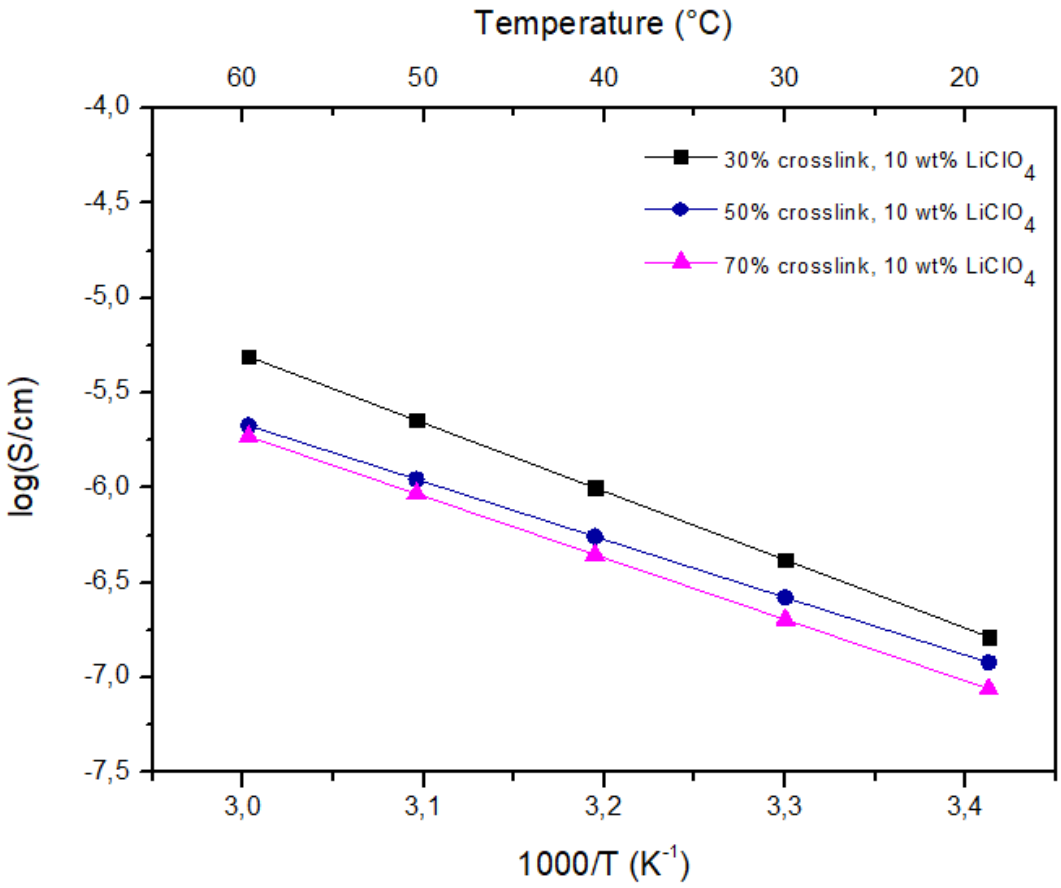

Graph 10: Temperature-dependent conductivity of the crosslinked G131 with PEGDE 200 g/mol

Since the PEGDE 200 g/mol is a short chain, the crosslinked network formed is tight. The movement of the polymer chains is thus limited in such a network. The ionic conductivity of three samples with different crosslinking percentages were tested. Only 10 wt % of $LiClO_4$ were added as the network with PEGDE 200 g/mol does not possess much space to dissolve and transport lithium ions. The ionic conductivity of the network crosslinked at 30, 50 and 70% with 10 wt % in $LiClO_4$ is displayed in Graph 10. The highest ionic conductivity is obtained with the sample crosslinked at 30%. An ionic conductivity of $4{,}9.10^{-6}$ $S.cm^{-1}$ is observed at 60 °C while that value decreased to $1{,}6.10^{-7}$ $S.cm^{-1}$ at 20 °C. The ionic conductivity for the other crosslinking percentages (50 and 70%) are shown in Table 14.

Table 14: Ionic conductivity at 60 and 20 °C of the crosslinked G131 with PEGDE 200 g/mol

Network with PEGDE 174 g/mol	**Ionic conductivity at 60°C ($S.cm^{-1}$)**	**Ionic conductivity at 20°C ($S.cm^{-1}$)**
30% crosslink	$4{,}9.10^{-6}$	$1{,}6.10^{-7}$
50% crosslink	$2{,}1.10^{-6}$	$1{,}2.10^{-7}$
70% crosslink	$1{,}9.\ 10^{-6}$	$8{,}7.10^{-8}$

A higher ionic conductivity is obtained when the crosslinking density is decreased. Indeed, with less crosslinking points, the polymer chains have more mobility, thus improving the lithium transport and ionic conductivity.

4.4.1.2. Network with PEGDE 500 g/mol

The ionic conductivity of the crosslinked G131 with PEGDE 500 g/mol is represented in the Graph 11, where the logarithm of the ionic conductivity (in S/cm) is plotted as function of 1000/temperature (K^{-1}). The sample tested contained different crosslinking percentages (30, 50, 70 and 100%) with 10 or 20 wt % of $LiClO_4$ added.

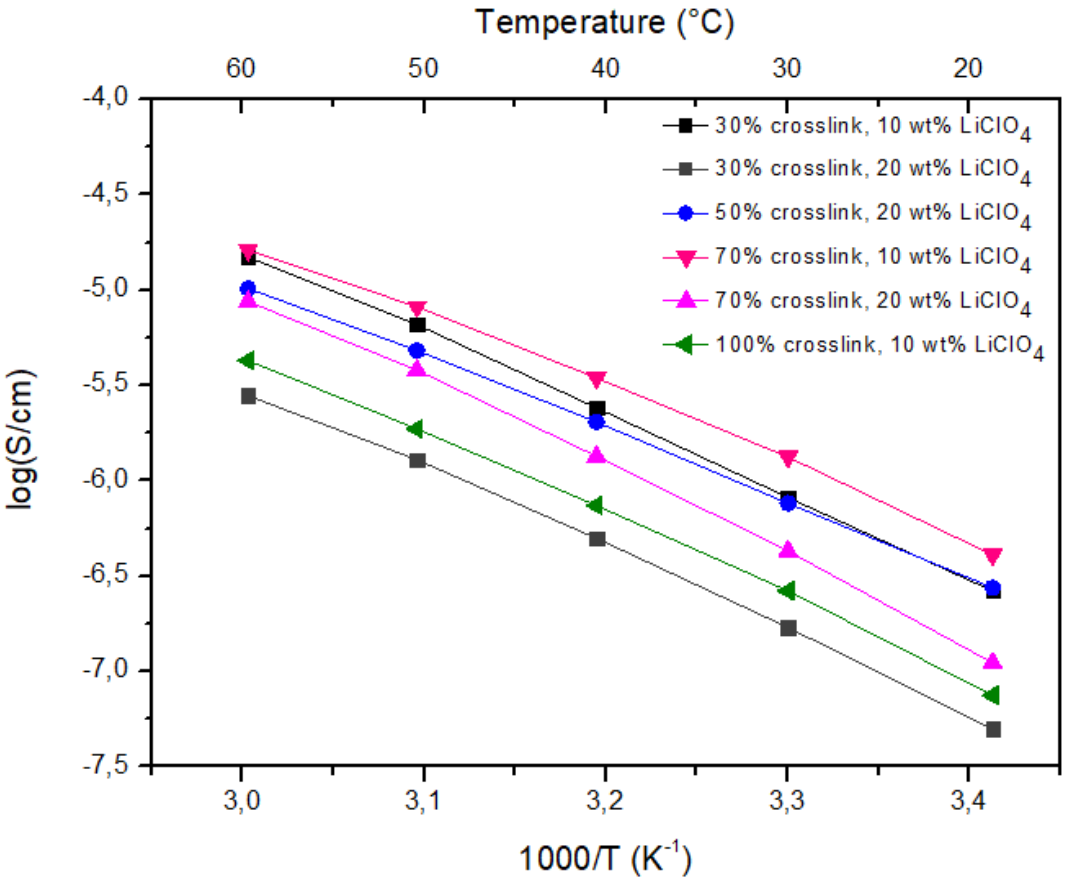

Graph 11: Temperature-dependent conductivity of the crosslinked G131 with PEGDE 500 g/mol

Just as for the crosslinked G131 with PEGDE 200 g/mol, we would expect that decreasing the crosslinking density would improve the ionic conductivity. However, the same relationship between crosslinking density and ionic conductivity cannot be found for the crosslinked G131 with PEGDE 500 g/mol. The highest ionic conductivity is obtained with the sample crosslinked at 70% with 10 wt % of $LiClO_4$. An ionic conductivity of $1{,}6.10^{-5}$ $S.cm^{-1}$ is observed at 60 °C while that value decreases to $2{,}6.10^{-7}$ $S.cm^{-1}$ at 20 °C. The ionic conductivity for the other crosslinking percentages (with 10 and 20 wt % of $LiClO_4$) are shown in Table 15.

Overall, the samples with 20 wt % in $LiClO_4$ gave a lower ionic conductivity than their 10 wt % counterparts (same crosslinking density). This can be explained by the fact that the network does not have enough space to dissolve a larger amount of lithium salt. It would certainly lead to the formation of aggregates, therefore diminishing the ionic conductivity compared to the same sample with 10 wt % of $LiClO_4$.

Why the less-crosslinked samples (30 and 50%) have a lower ionic conductivity than the 70% is still unclear.

Table 15: Ionic conductivity at 60 and 20 °C of the crosslinked G131 with PEGDE 500 g/mol

Network with PEGDE 500 g/mol	**Ionic conductivity at 60°C ($S.cm^{-1}$)**	**Ionic conductivity at 20°C ($S.cm^{-1}$)**
30% crosslink, 10 wt% $LiClO_4$	$1,5.10^{-5}$	$2,6.10^{-7}$
30% crosslink, 20 wt% $LiClO_4$	$2,8.10^{-6}$	5.10^{-8}
50% crosslink, 20 wt% $LiClO_4$	1.10^{-5}	$2,8.10^{-7}$
70% crosslink, 10 wt% $LiClO_4$	$1,6.10^{-5}$	$4,1.10^{-7}$
70% crosslink, 20 wt% $LiClO_4$	$8,7.10^{-6}$	$1,2.10^{-7}$
100% crosslink, 10 wt% $LiClO_4$	$4,3.10^{-6}$	$7,5.10^{-8}$

4.4.1.3. Network with PEGDE 1100 g/mol

The ionic conductivity of the crosslinked G131 with PEGDE 1100 g/mol is shown in the Graph 12, where the logarithm of the ionic conductivity (in S/cm) is plotted as function of 1000/temperature (K^{-1}). The sample tested contained different crosslinking percentages (30, 50, 70 and 100%) with 10 or 20 wt % of $LiClO_4$ added.

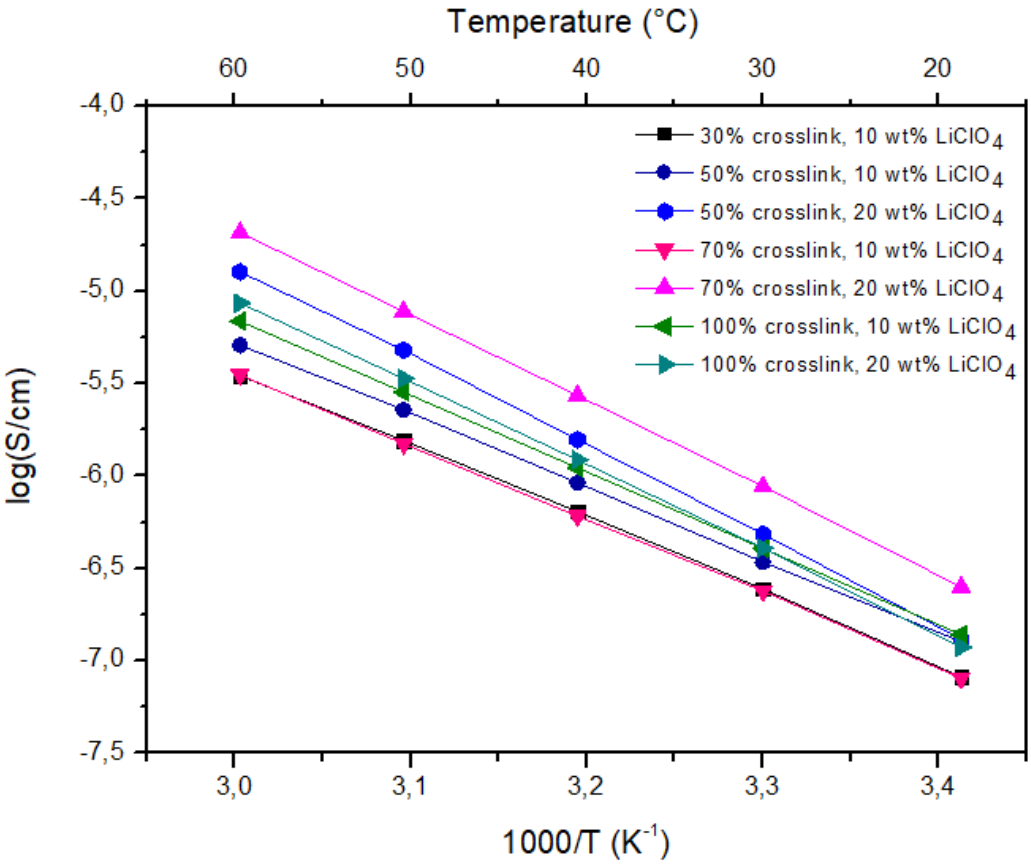

Graph 12: Temperature-dependent conductivity of the crosslinked G131 with PEGDE 1100 g/mol

The highest ionic conductivity is obtained with the sample crosslinked at 70% with 20 wt % of $LiClO_4$. An ionic conductivity of $2{,}1.10^{-5}$ $S.cm^{-1}$ is observed at 60 °C while that value drops to $2{,}5.10^{-7}$ $S.cm^{-1}$ at 20 °C. The ionic conductivity for the other crosslinking percentages (with 10 and 20 wt % of $LiClO_4$) are represented in Table 16.

Similarly to the crosslinked G131 with PEGDE 500 g/mol, the network crosslinked at 70% gave the best the best ionic conductivity.

The difference between the crosslinked network with PEGDE 500 and 1100 g/mol, is that the samples with 20 wt % in $LiClO_4$ show this time a higher ionic conductivity than their 10 wt % counterparts (same crosslinking density). As the crosslinker chains are longer (PEGDE 1100 g/mol), a wider network is formed. The network contains more space, helping to dissolve a higher amount of lithium salt while avoiding the formation of aggregates.

Table 16: Ionic conductivity at 60 and 20 °C of the crosslinked G131 with PEGDE 1100 g/mol

Network with PEGDE 1099 g/mol	**Ionic conductivity at 60°C ($S.cm^{-1}$)**	**Ionic conductivity at 20°C ($S.cm^{-1}$)**
30% crosslink, 10 wt% $LiClO_4$	$3{,}5.10^{-6}$	$8{,}2.10^{-8}$
50% crosslink, 10 wt% $LiClO_4$	$5{,}1.10^{-6}$	$1{,}3.10^{-7}$
50% crosslink, 20 wt% $LiClO_4$	$1{,}3.10^{-5}$	$1{,}3.10^{-7}$
70% crosslink, 10 wt% $LiClO_4$	$3{,}5.10^{-6}$	8.10^{-8}
70% crosslink, 20 wt% $LiClO_4$	$2{,}1.10^{-5}$	$2{,}5.10^{-7}$
100% crosslink, 10 wt% $LiClO_4$	$6{,}9.10^{-6}$	$1{,}4.10^{-7}$
100% crosslink, 20 wt% $LiClO_4$	$8{,}6.10^{-6}$	$1{,}2.10^{-7}$

4.4.1.4. Network with PEGDE 2000 g/mol

The ionic conductivity at 20°C of the crosslinked G131 with PEGDE 2000 g/mol is shown in the Graph 13. Only the network crosslinked at 30 and 70% with 10 wt % in $LiClO_4$ were tested at 20°C.

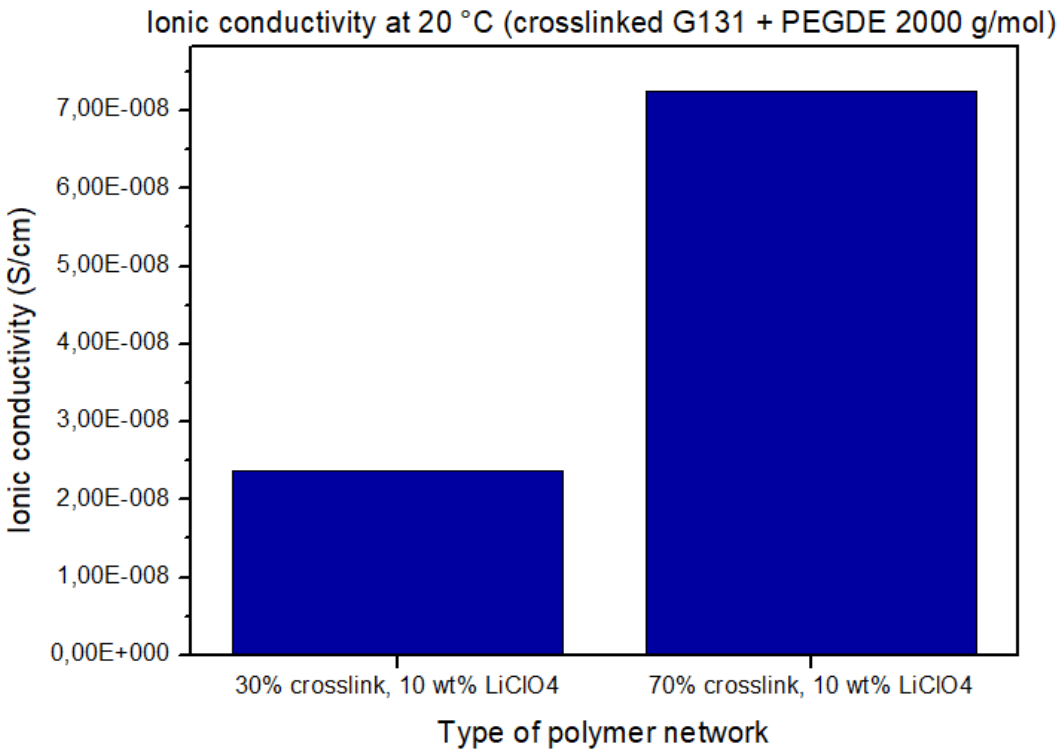

Graph 13: Comparison of the ionic conductivity at 20°C for different crosslinking %

The highest ionic conductivity is obtained with the sample crosslinked at 70% with 10 wt % of $LiClO_4$. An ionic conductivity of $7{,}2.10^{-8}$ $S.cm^{-1}$ is observed at 20 °C for this network (as reported in Table 17). Just as for the networks with PEGDE 500 and 1100 g/mol, the network crosslinked at 70% gave the best result. However, with PEGDE 2000 g/mol, the chains are quite long, leading to a loose network even for the system crosslinked at 70%. This explains why the ionic conductivity of the networks with PEGDE 2000 g/mol are lower than for the networks with PEGDE 500 and 1100 g/mol.

Table 17: Ionic conductivity at 20 °C of the crosslinked G131 with PEGDE 2000 g/mol

Network with PEGDE 2000	**Ionic conductivity at 20°C ($S.cm^{-1}$)**
30% crosslink, 10 wt% $LiClO_4$	$2{,}4.10^{-8}$
70% crosslink, 10 wt% $LiClO_4$	$7{,}2.10^{-8}$

4.4.1.5. Comparison of the different PEGDE

The best ionic conductivity obtained from each network (with PEGDE 200, 500 and 1100 g/mol) is represented in the Graph 14. The logarithm of the ionic conductivity (in S/cm) is plotted as function of 1000/temperature (K^{-1}).

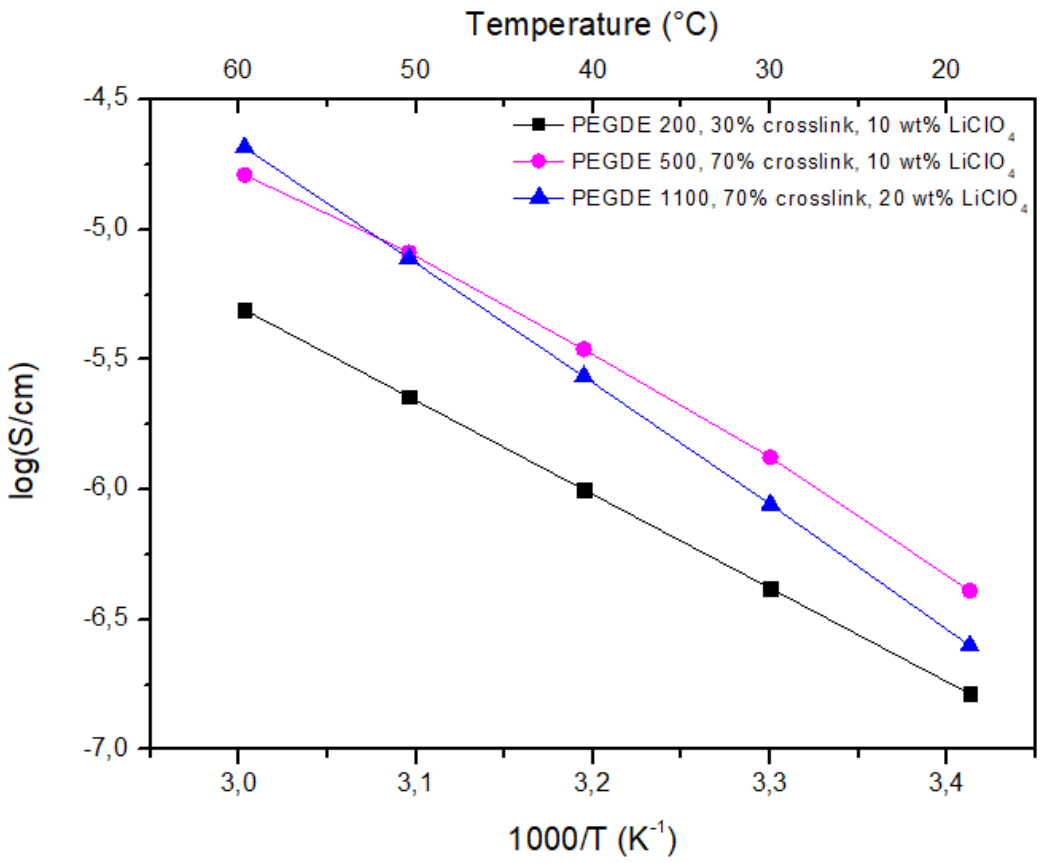

Graph 14: Temperature-dependent conductivity of the crosslinked G131 with PEGDE 200 g/mol, 500 g/mol and 1100 g/mol

The impact of the PEGDE molecular weight on the ionic conductivity was compared by taking the best sample of the networks with PEGDE 200, 500 and 1100 g/mol. Table 18 reports the ionic conductivity at 60 °C and 20 °C of the best samples. The polymer network with PEGDE 500 g/mol possesses the highest ionic conductivity at 20°C, followed by the network with PEGDE 1100 g/mol, then PEGDE 200 g/mol. The crosslinked G131 with PEGDE 500 g/mol has the best ionic conductivity among the different PEGDE as it has the optimal length of crosslinker chain. A shorter crosslinker chain like PEGDE 200 g/mol will form a tight network where the mobility of the chains is restricted (thus diminishing the ionic conductivity). On the other hand, a longer crosslinker chain like PEGDE 1100 g/mol will lead to a loose network.

Table 18: Ionic conductivity at 60 and 20 °C of the crosslinked G131 with different PEGDE

Network with different PEGDE	**Ionic conductivity at 60°C ($S.cm^{-1}$)**	**Ionic conductivity at 20°C ($S.cm^{-1}$)**
PEGDE 174, 30% crosslink, 10 wt% $LiClO_4$	$4{,}9.10^{-6}$	$1{,}6.10^{-7}$
PEGDE 500, 70% crosslink, 10 wt% $LiClO_4$	$1{,}6.10^{-5}$	$4{,}1.10^{-7}$
PEGDE 1099, 70% crosslink, 20 wt% $LiClO_4$	$2{,}1.10^{-5}$	$2{,}5.10^{-7}$

To conclude, after investigating the impact of the crosslinking density and the MW of the crosslinker, the highest ionic conductivity was found with the crosslinked G131 with PEGDE 500 g/mol (70% crosslink with 10 wt % of $LiClO_4$). Our results emphasize the importance of the network structure on the ionic conductivity. In order to observe the best ionic conductivity, the network should not be too highly crosslinked (70% of crosslinking seems to be the best value) and the distance between crosslinking nodes should not be too small or too large (the use of the PEGDE 500 gave the best value). At this stage, it is not clear to understand how these two parameters affect the mobility of lithium ions.

5. Conclusion and outlook

This master thesis focused on the synthesis and characterization of solid polymer electrolytes with a vitrimer behaviour. The aim of this work was to improve the ionic conductivity of the crosslinked network (G131 with PEGDE). Two parameters were played on to attain that goal. First of all, the molecular weight of the crosslinker (PEGDE) was changed to observe the impact on the ionic conductivity. Four different MW of PEGDE were tested: 200, 500, 1100 and 2000 g/mol. Then, the impact of the crosslinking density was observed by decreasing the crosslinking percentage (100, 70, 50 and 30% crosslink).

The thermal characterization of the polymer networks showed that the crosslinking density and MW of the PEGDE have little influence on the glass transition temperature. However, the addition of $LiClO_4$ results in T_g shifts from -50 °C to -35 °C

The self-healing ability of the polymer network with PEGDE 500 g/mol was assessed by optical microscopy and tensile test. While almost no self-healing could be observed by optical microscopy for the different crosslinking percentages, the tensile test showed around 30% and 37% of self-healing after 24 hours for the 70% and 30% crosslinked network respectively. A lower crosslinking density improves the self-healing ability as the polymer chains can move more freely to other chains for the disulfide metathesis. The self-healing not exceeding 37% after 24 hours could be because some S-S bonds can undergo oxidation when exposed to oxygen (O_2) and that they are self-healing faster within the same cut part. To validate this hypothesis, the self-healing will be assessed under inert atmosphere.

The best ionic conductivity is obtained with the 70% crosslinked G131 with PEGDE 500 g/mol containing 10 wt % of $LiClO_4$. This sample is the right compromise between the crosslinking density and the length between crosslinking nodes. With a high crosslinking density (100%) and a tight network (PEGDE 200 g/mol), the polymer chains have little mobility, thus decreasing the ionic conductivity. On the other hand, low crosslinking density (50 and 30%) and loser networks (formed with PEGDE 1100 or 2000 g/mol) lead to lower ionic conductivity although better chain mobility is expected. It seems that there is a trade-off to find in the structure of the network that should not be too stiff nor too loose. A detailed rheological characterization of the different types of networks investigated here could bring some new piece of information to understand our observations. In that respect, optimal ionic conductivity could be maybe reached within a certain range of rheological properties. Those

experiments could be performed in the near future. Those new data could also help to understand more clearly the self-healing abilities of our networks.

Further analysis, such as the preparation of a catholyte could be performed on that sample with the best ionic conductivity. The catholyte is a cathode containing the SPE as binder. This improves the solid electrolyte/cathode interface and increases the ionic conductivity.

6. Bibliography

[1] *Paris Suspends Electric Bus Fleet after Two Fires*. 29 April 2022. Le Monde.Fr. 19 February 2023. < https://www.lemonde.fr/en/france/article/2022/04/29/paris-suspends-electric-bus-fleet-after-two-fires_5981956_7.html.>.

[2] *Lithium-Ion Battery Fires: Myth vs. Reality*. n.d. 19 February 2023. <https://www.tuvsud.com/en-us/resource-centre/stories/lithium-ion-battery-fires-myth-vs-reality.>.

[3] Y. Chen *et al.* «A Review of Lithium-Ion Battery Safety Concerns: The Issues, Strategies, and Testing Standards.» *Journal of Energy Chemistry* 59 (2021): 83-99.

[4] *Lithium-Ion Battery*. n.d. Clean Energy Institute. 27 February 2023. <https://www.cei.washington.edu/education/science-of-solar/battery-technology/>.

[5] X. Duan, et al. "Recycling of Lithium Batteries—A Review." *Energies* 15.5 (2022): 1611.

[6] *European Climate Law*. n.d. 7 March 2023. <https://climate.ec.europa.eu/eu-action/european-green-deal/european-climate-law_en>.

[7] *Brussels to Ban Diesel Cars from 2030, Petrol Cars from 2035* . 25 June 2021. POLITICO. 7 March 2023. <https://www.politico.eu/article/brussels-wants-to-start-banning-gas-guzzling-cars-from-2030/>.

[8] W. Zhao, J. Yi, P. He, and H. Zhou. «Solid-State Electrolytes for Lithium-Ion Batteries: Fundamentals, Challenges and Perspectives .» *Electrochem. Energ. Rev.* 2.4 (2019): 574-605.

[9] *Battery | Electronics*. 26 december 2022. Britannica. 20 February 2023. <https://www.britannica.com/technology/battery-electronics>.

[10] J. Shepard, *The Difference between Primary and Secondary Battery Chemistries*. 8 July 2021. Battery Power Tips. 17 April 2023. <https://www.batterypowertips.com/difference-between-primary-secondary-battery-chemistries-faq/>.

[11] A. Dutta, et al. “ A Comprehensive Review on Batteries and Supercapacitors: Development and Challenges since Their Inception.” *Energy Storage* 5.1 (2023).

[12] *Battery Working Principe, Work?* n.d. Electrical4U. 23 April 2023. <https://www.electrical4u.com/battery-working-principle-of-batteries/>.

[13] A. Vlad, *LCHM2260 Electrochemical energy storage*. Louvain-la-Neuve, 2022.

[14] *Why Is Lithium Used In Batteries? Facts You Need To Know* . 5 Augustus 2022. Raunik GreenTech Pvt Ltd . 25 April 2023. <https://www.raunik.com/why-is-lithium-used-in-batteries/ >.

[15] *How does a lithium-Ion battery work?* 23 September 2019. Let’s Talk Science. 25 April 2023. <https://letstalkscience.ca/educational-resources/stem-in-context/how-does-a-lithium-ion-battery-work>.

[16] *Where do batteries come from? And where do they go?* 7 March 2023. SoundGuys. 10 April 2023. <https://www.soundguys.com/lithium-ion-batteries-environmental-impact-56781>.

[17] P. Zhu, D. Gastol, J. Marshall, R. Sommerville, V. Goodship, and E. Kendrick. “A review of current collectors for lithium-ion batteries.” *Journal of Power Sources* 485 (2021): 229321.

[18] S. Jin et. al., “ A comprehensive review on the recycling of spent lithium-ion batteries: Urgent status and technology advances.” *Journal of Cleaner Production* 340 (2022): 130535.

[19] Z. Zhang, P. Arora, et al. «Battery Separators.» *Chem. Rev.* 104.10 (2004): 4419-4462.

[20] *Novel lithium-metal batteries will drive the switch to electric cars*. s.d. MIT Technology Review. 5 May 2023. <https://www.technologyreview.com/2021/02/24/1018102/lithium-metal-batteries-electric-vehicle-car/>.

[21] J. Schnell et. al., “ All-solid-state lithium-ion and lithium metal batteries – paving the way to large-scale production .” *Journal of Power Sources* 382 (2018): 160-175.

[22] X. Zhang, Y. Yang, and Z. Zhou. « Towards practical lithium-metal anodes.» *Chem. Soc. Rev.* 49.10 (2020): 3040-3071.

[23] X.-B. Cheng, R. Zhang, C.-Z. Zhao, and Q. Zhang. " Toward Safe Lithium Metal Anode in Rechargeable Batteries: A Review." *Chem. Rev.* 117.15 (2017): 10403-10473.

[24] W. Zhao et al. «Solid-State Electrolytes for Lithium-Ion Batteries: Fundamentals, Challenges and Perspectives .» *Electrochemical Energy Reviews* 2.4 (2019): 574-604.

[25] H. Zhang et. al., «Single lithium-ion conducting solid polymer electrolytes: advances and perspectives.» *Chem. Soc. Rev.* 46.3 (2017): 797-815.

[26] G. Piana, *Electrolyte solide innovant à base de liquides ioniques pour microaccumulateurs au lithium: réalisation par voie humide et caractérisation des propriétés de transport*. Thesis. Paris, 2016.

[27] H. Aziam, B. Larhrib, C. Hakim, N. Sabi, H. Ben Youcef, and I. Saadoune. " Solid-state electrolytes for beyond lithium-ion batteries: A review." *Renewable and Sustainable Energy Reviews* 167 (2022): 112694.

[28] V. P. Hoang Huy, S. So, and J. Hur. "Inorganic Fillers in Composite Gel Polymer Electrolytes for High-Performance Lithium and Non-Lithium Polymer Batteries." *Nanomaterials* 11.3 (2021): 614.

[29] J. Zheng et al. "Vitrimers: Current research trends and their emerging applications." *Materials Today* 51 (2021): 586-625.

[30] J. M. Winne, L. Leibler, and F. E. Du Prez. "Dynamic covalent chemistry in polymer networks: a mechanistic perspective." *Polym. Chem.* 10.45 (2019): 6091-6108.

[31] F. Ling et. al., «Compatibility driven self-strengthening during the radical-responsive remolding process of poly-isoprene vitrimers.» *J. Mater. Chem.* 7.44 (2019): 25324-25332.

[32] Y. H. Jo et. al., "Self-Healing Solid Polymer Electrolyte Facilitated by a Dynamic Cross-Linked Polymer Matrix for Lithium-Ion Batteries." *Macromolecules* 53.3 (2020): 1024-1032.

[33] S. Nevejans, N. Ballard, J. I. Miranda, B. Reck, and J. M. Asua,. «The underlying

mechanisms for self-healing of poly(disulfide)s.» *Phys. Chem. Chem. Phys.* 18.39 (2016): 27577-27583,.

[34] Z. Lei, H. Xiang, Y. Yuan, M. Rong, and M. Zhang. “Room-Temperature Self-Healable and Remoldable Cross-linked Polymer Based on the Dynamic Exchange of Disulfide Bonds.” *Chem. Mater.* 26.6 (2014): 2038-2046.

[35] W. Denissen, J. M. Winne, and F. E. Du Prez. “ Vitrimers: permanent organic networks with glass-like fluidity.” *Chem. Sci.* 7.1 (2016): 30-38.

[36] Nazmutdinova, Elina. *Synthesis and characterization of solid electrolytes based on vitrimer-like ionically-conducting polymers*. Master thesis. Louvain-la-Neuve, 2021.

[37] A. O. Konuray, X. Fernández-Francos, et X. Ramis. «Analysis of the reaction mechanism of the thiol–epoxy addition initiated by nucleophilic tertiary amines.» *Polym. Chem.* 8.38 (2017): 5934-5947.

[38] Garcia, Y. *LCHM2122 - Physical Methods for the Analysis of Solids*. Louvain-la-Neuve, 2022.

[39] *Chip DSC 10 – Polymères - PET*. 10 September 2021. Linseis Messgeräte GmbH. 15 May 2023. < https://www.linseis.com/fr/votre-industrie/polymeres/chip-dsc-10-polymeres-pet/>.

[40] X. Liu and W. Yu. “Evaluating the thermal stability of high performance fibers by TGA.” *J. Appl. Polym. Sci.* 99.3 (2006): 937-944.

[41] A. Borhade, T. Kshirsagar, A. Dholi, et J. Agashe. “Removal of Heavy Metals Cd 2+ , Pb 2+ , and Ni 2+ From Aqueous Solutions Using Synthesized Azide Cancrinite, Na 8 [AlSiO 4] 6 (N 3) 2.4 (H 2 O) 4.6.” *J. Chem. Eng. Data* 60.3 (2015): 586-593.

[42] D. Drummer, A. Seefried, and S. Meister. « Characterization of Material Stiffness on Injection Moulded Microspecimens Using Different Test Methods.» *Advances in Materials Science and Engineering* 2014 (2014): 1-8.

[43] D. Schäfer, F. Lisdat et al. “The use of electrochemical impedance spectroscopy for biosensing .” *Anal Bioanal Chem* 391.5 (2008): 1555-1567.

[44] N. Meddings et. al., “Application of electrochemical impedance spectroscopy to

commercial Li-ion cells: A review." *Journal of Power Sources* 480 (2020): 228742.

[45] H. S. Magar, R. Y. A. Hassan, and A. Mulchandani. "Electrochemical Impedance Spectroscopy (EIS): Principles, Construction, and Biosensing Applications." *Sensors* 21.19 (2021): 6578.

[46] J. Abrantes, D. Ribeiro et al. "Application of electrochemical impedance spectroscopy (EIS) to monitor the corrosion of reinforced concrete: A new approach." *Construction and Building Materials* 111 (2016): 98-104.

[47] W. Kao-ian, R. Pornprasertsuk, P. Thamyongkit, T. Maiyalagan, and S. Kheawhom,. "Rechargeable Zinc-Ion Battery Based on Choline Chloride-Urea Deep Eutectic Solvent." *J. Electrochem. Soc.* 166.6 (2019): 1063-A1069.

[48] "RAMAN Band Correlation Table." n.d. 27 May 2023. <https://www.chem.uci.edu/~dmitryf/manuals/Raman%20correlations.pdf>.

[49] J. Maranas, S. Fullerton-Shirey et al. «Effect of LiClO4 on the Structure and Mobility of PEO-Based Solid Polymer Electrolytes.» *Macromolecules* 42.6 (2009): 2142-2156.

Appendices

Table of content

A. Appendix A – Film formation by dropcasting

The preparation of a solution with the polymer network and the lithium salt is identical to the method with Teflon mould. But instead of pouring that mixture in a mould, a few drops are deposited with a pipette Pasteur or a micropipette on a stainless steel. After letting the THF evaporate for 1 hour, another layer of drops is applied on the stainless steel. Around 2~4 layers are usually added. The rest of the THF is evaporated overnight, and the stainless steel with the SPE is then cured in the oven under vacuum at 60 °C for 5 hours. This method was replaced by the one with Teflon moulds because the films obtained were quite thick (around 300-400 µm), inhomogeneous, and with bubbles trapped inside the SPE.

Figure 28: SPE films obtained by dropcasting

B. Appendix B – DSC graphs

B.1 Heating and cooling DSC curves

The complete DSC graph (with 2 heating curves and one cooling curve) of the crosslinked G131 with PEGDE 500 g/mol (crosslinked at 100%) is represented in Graph 15. No melting or crystallization peaks are observed for the crosslinked polymer network.

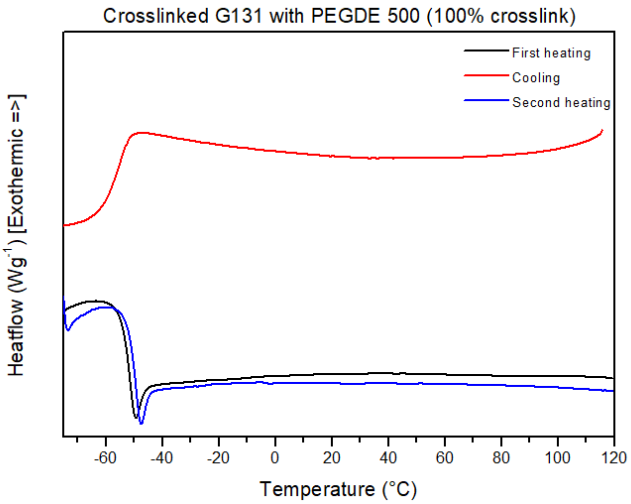

Graph 15: Complete DSC curves of the crosslinked G131 with PEGDE 500 g/mol (100% crosslink)

B.2 Comparison with the reagents

The crosslinked polymer network was compared with the reagents (thioplast G131 and PEGDE 1100 g/mol) through a DSC analysis.

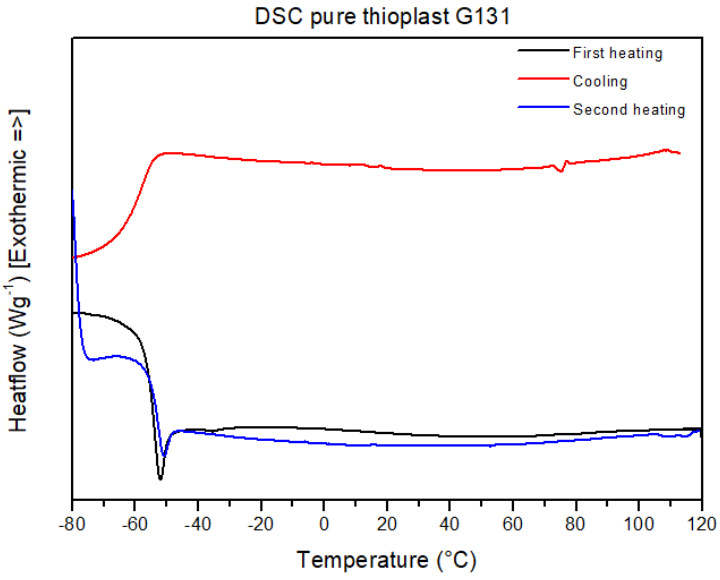

Graph 16: Complete DSC curves of the pure thioplast G131

The pure thioplast G131 showed a glass transition at -54 °C but no crystallization or melting peaks.

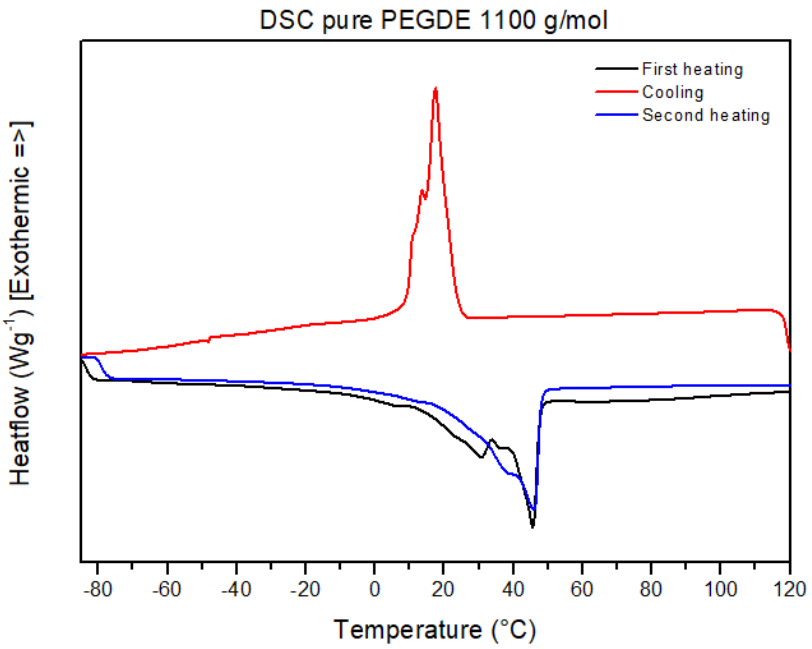

Graph 17: Complete DSC curves of the pure PEGDE 1100 g/mol

Pure PEGDE 1100 g/mol is a semi-crystalline polymer with a T_g at -76 °C, the melting temperature at 45 °C and crystallization temperature at 18 °C.

C. Appendix C – Optical microscopy

For the crosslinked G131 with PEGDE 1100 g/mol (30% crosslink), the width of the cut performed on the sample became larger after 24 hours. The images and width of the cut after 0 and 24 hours are reported in Table 19. Even though this sample did not completely heal after 24 hours, self-healing can be observed (beginning at the bottom of the sample and going to the top of the sample). The initial width at the bottom of the sample was 1297 µm whereas that gap decreased to 171 µm after 24 hours.

Table 19: Optical images of the network crosslinked at 30% with PEGDE 1100 g/mol

After 0 hours	**After 24 hours**
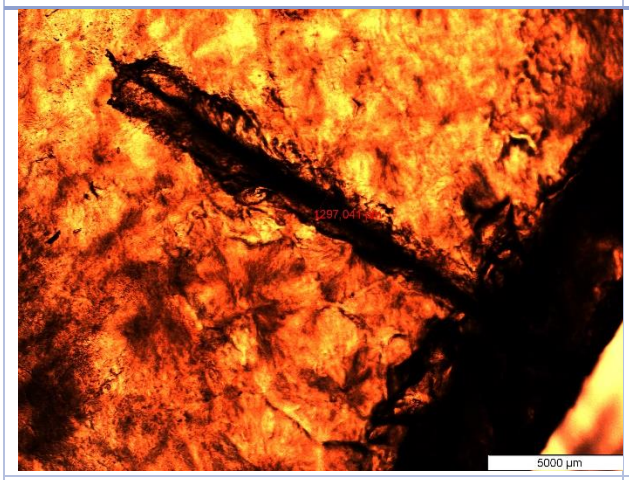	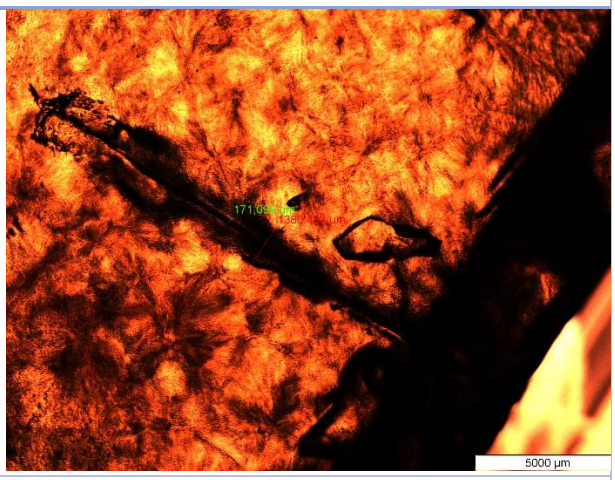
Distance: 1297 µm	**Distance:** 1380 µm

UNIVERSITÉ CATHOLIQUE DE LOUVAIN
Faculté des sciences
Place des sciences, 2 bte L6.06.01, 1348 Louvain-la-Neuve, Belgique | **www.uclouvain.be/sc**